Ann. Rev. Fluid Mech. 1981. 13:457–515

ORGANIZED MOTION IN TURBULENT FLOW

*8184

Brian J. Cantwell
Department of Aeronautics and Astronautics, Stanford University, Stanford, California 94305

I INTRODUCTION

In nearly every area of fluid mechanics, our understanding is limited by the onset or presence of turbulence. Although recent years have seen a great increase in our physical understanding, a predictive theory of turbulent flow has not yet been established. Aside from certain results that can be derived through dimensional reasoning, it is still not possible to solve from first principles the simplest turbulent flow with the simplest conceivable boundary conditions. Our continuing inability to make accurate, reliable predictions seriously limits the technological advancement of aircraft design, design of turbomachinery, combustors, mixers, and a wide variety of other devices that depend on fluid motion for their operation.

Anyone who is introduced to the subject of turbulence for the first time quickly encounters the decomposition of the unsteady flow first proposed by Osborne Reynolds in 1895. Various flow variables are divided into a mean and fluctuating part, and upon substitution into the Navier-Stokes equations the result is a system of equations identical in form to the original system except for convective stress terms, which arise from averaging products of velocity fluctuations. In order to close the system of equations, a second relation is needed between the convective stresses and the mean velocity field. Until recently, much theoretical and experimental effort was focused on finding relationships that could be applied to larger and larger classes of mean flows with the ultimate hope of finding a universal constitutive relation for "turbulent fluid." There was never any guarantee that such a relation actually exists and the goals of this effort remain largely unrealized. Hope for a universal turbulence model has been slowly replaced by the growing

realization that the formulation of an adequate theory will require a greatly improved understanding of the physics of turbulent motion.

Recently there has been an increased emphasis on direct analysis or measurement of complex unsteady flow fields under rather restricted conditions. Remarkably elaborate and detailed experimental and analytical studies have been made possible by advances in electronic and optical instrumentation and computational hardware and software. An extremely important element in current experimental research is a renewed emphasis on the use of flow visualization and a widespread awareness that flow visualization can play a very broad role in improving our physical understanding of complicated turbulent phenomena (Kline 1978). Today, flow visualization, as an experimental tool for identifying new flow structure and as a conceptual tool for reducing complex flow processes to simple pictures, lies at the heart of what may eventually become a genuinely new understanding of turbulent flow.

In order to understand current research trends, it is helpful to review the way in which our physical picture of turbulence has evolved over the past several decades. To an investigator of the 1920s or 1930s, turbulence was essentially a stochastic phenomenon having a well-defined and repeatable mean superimposed on a randomly fluctuating velocity field. The motion was characterized by a wide range of scales limited in size only by the overall dimensions of the flow. This picture of randomly interacting scales led to the semi-empirical theories of Prandtl (1925) and Taylor (1915, 1932) in which convective stresses were connected to the mean flow by an effective eddy viscosity[1] or mixing length. Although the concept of an eddy played a central role in constructing mathematical models of turbulence, it was essentially an abstraction and early work on turbulence is marked by a singular lack of any attempt to sketch or schematically visualize turbulent motion.

The complexity of inhomogeneous turbulence led Taylor (1935) to study a homogeneous and isotropic field of turbulence which is initiated by some uniformly distributed stirring mechanism and decays with time. Interest in the statistical theory of turbulence dominated the field throughout the 1940s, and the early development of this theory, though usually attributed primarily to Kolmogorov (1941), also includes important contributions from Onsager (1945), Von Weizsacker (1948), Kovasznay (1948), Heisenberg (1948a, b), and Chandrasekhar (1949). For a review and useful early perspective on the turbulence problem see Liepmann (1952).

Considerations of the spectral evolution of homogeneous and isotropic turbulence led to the important observation that the energy-containing structure of isotropic turbulence does not depend directly on

[1]A concept introduced by Boussinesq in 1877.

the value of the fluid viscosity. It was observed that if the Reynolds number is high enough to insure turbulence then the energy-containing flow structure is similar at all higher Reynolds numbers. In addition it was observed that if the Reynolds number is large enough, the zone of dissipation and the zone of production of turbulent energy will be widely separated in wave-number space. In this case the small-scale motion is in a state of local isotropic equilibrium. Implicit in the idea of local isotropy is the assumption that the direct coupling between large- and small-scale motions is weak and that the behavior of small eddies is universally the same from flow to flow.

A new element was added to the physical picture of turbulence by Corrsin (1943) and Townsend (1947) who showed that the outer edges of turbulent shear flows, specifically wakes and jets, are only intermittently turbulent. The intermittent nature of turbulence was confirmed by Corrsin & Kistler (1954) and Klebanoff (1954) and by the middle of the 1950s the physical picture of turbulence had pretty much evolved to the state illustrated by several examples in Figure 1. This picture, which is attributed primarily to Townsend (1956), combines the laminar superlayer of Corrsin & Kistler (1954) with a field of turbulent fluid of nearly uniform intensity. The dynamical characteristics of this field are similar to the characteristics of isotropic turbulence. The turbulent fluid is moved about by the slow convective motion of a system of large eddies whose dimensions are comparable to the width of the flow and much larger than the scale of the eddies containing most of the turbulent energy. Outside the turbulent interface, the motion is unsteady, irrotational potential flow induced by movement at the boundary.

Townsend viewed the large eddies and small-scale turbulence as the main features of what he called a double structure, and he emphasized the importance of the large eddies in controlling transport.[2] He also realized that the large eddies ought to have a quasi-deterministic form and attempted, really for the first time, to draw a picture of the large-eddy motion. Attempts to produce such a picture usually took the form of inferences based on the long-time-averaged spatial-correlation tensor

$$R_{ij}(\mathbf{x}, \xi) = \overline{u_i(\mathbf{x}, t)u_j(\mathbf{x}+\xi, t)} \tag{1}$$

measured in an Eulerian frame. Extensive correlation measurements by Grant (1958) in the far wake of a circular cylinder ($x/D=533$) were used by Payne & Lumley (1967) to produce the structure shown in

[2] Interestingly, the discussion of double structure does not appear in Townsend's second edition (1976). Apparently influenced by recent experimental evidence in boundary layers and channels, Townsend was moved to delete the discussion of double structure from the new text.

Figure 2*a*. More recently, Townsend (1970) inferred the double-roller large-eddy structure shown in Figure 2*b* for a general shear flow and the double-cone structure shown in Figure 2*c* for a wall-bounded shear flow (Townsend 1976).

This approach to the large-eddy structure through the Eulerian spatial-correlation tensor is rooted in the stochastic random-scales picture of "turbulent fluid" and suffers from a number of shortcomings. The first and most obvious is that there does not exist a unique relationship between the correlation tensor and the unsteady flow that produces it. A second shortcoming is that the correlated portion of the signal associated with the passage of an organized and repeatable motion will be degraded by other contributions to the total signal. This may lead to results that emphasize certain mechanisms while ignoring others, and that may be erroneous or incomplete even in a qualitative sense. Early correlation measurements taken in mixing layers failed spectacularly to reveal the large spanwise eddies now known to dominate this flow. A third shortcoming is that the averaging point does not propagate with the disturbances that are responsible for the correlated portion of the signal. A Lagrangian averaging process might reveal quite a different structure from the Eulerian average. A final shortcoming is that the correlation method leads to an incomplete picture of the flow with vortex lines left unclosed and schematic patterns of lines that often defy definition. In short, the method offers no information about how arrays of moving large eddies are laced together to complete the flow field.

Beginning in the early 1960s, experiments were performed that began to change the view of turbulence just summarized. The last twenty years of research on turbulence have seen a growing realization that the transport properties of most turbulent shear flows are dominated by large-scale vortex motions that are not random. The form, strength, and scale of these organized motions vary from flow to flow and methods used to identify them are as varied as the motions themselves.

II ORGANIZED MOTION IN THE TURBULENT BOUNDARY LAYER

(a) Motivation

It is remarkable that the earliest observations of organized motion were made in the turbulent boundary layer along a wall where the motion is most complex. At least part of the reason is simply that this is the flow that has historically received the greatest attention because of its technological importance and would therefore be the most likely one to reveal

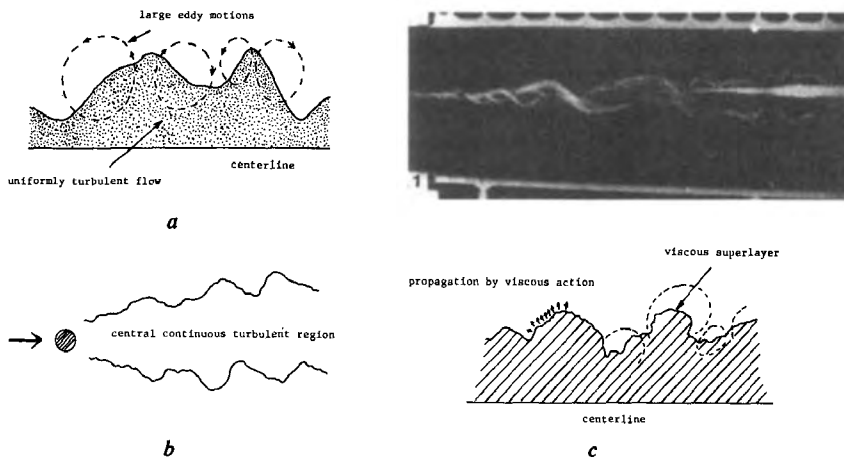

Figure 1 Several conceptual views of turbulent flow. (*a*) Sketch of a jet flow from Townsend (1956); (*b*) and (*c*) Sketches of a wake flow from Hinze (1959).

its structure first. However, another reason has to be related to the fascinating and compelling mean-flow behavior that the boundary layer exhibits. To a good approximation, the mean velocity profile of a turbulent boundary layer may be divided into three parts (see Figure 3*b*).

O–A: Viscous sublayer $0 \leqslant y^+ \lesssim 7$

$$y^+ = u^+. \tag{2}$$

A–B: Buffer layer $7 \lesssim y^+ \lesssim 30$. Several relations are available for this region. An implicit formula due to Spalding (1961) which matches (2) and (4) is

$$y^+ = u^+ + e^{-Kc}\left\{e^{Ku^+} - 1 - Ku^+ - \frac{1}{2}(Ku^+)^2 - \frac{1}{6}(Ku^+)^3\right\} \tag{3}$$

B–C–D: Logarithmic and outer layer $30 \lesssim y^+ \leqslant \delta^+$. An empirical formula that works well for a variety of pressure gradients is (Coles 1956)

$$u^+ = \frac{1}{K}\ln y^+ + C + \frac{\Pi(x)}{K} 2\sin^2\left(\frac{\pi}{2}\frac{y^+}{\delta+}\right) \tag{4}$$

where

$$y^+ = \frac{yu^*}{\nu}, \delta^+ = \frac{\delta u^*}{\nu}, \tag{5}$$

$$u^+ = u/u^* \tag{6}$$

and

$$u^* = \sqrt{\frac{\tau_\omega}{\rho}} \tag{7}$$

where

$$\tau_\omega = \mu \frac{\partial u}{\partial y}\bigg|_{y=0}. \tag{8}$$

The skin-friction coefficient is

$$C_f = \frac{\tau_\omega}{\frac{1}{2}\rho u_\infty^2} = 2\left(\frac{u^*}{u_\infty}\right)^2. \tag{9}$$

The profile (4) is determined by the two empirical constants K and C and the function $\Pi(x)$. Typical values are $K=0.4$ and $C=5.0$. The pressure gradient determines $\Pi(x)$. For $dP/dx=0$, $\Pi=0.62$. General features of the structure of the boundary layer are usually described in terms of wall variables (u^*, ν) or outer variables (u_∞, δ), although it is well to keep in mind that they are not independent quantities. In particular, the boundary-layer thickness δ is determined from the other three. From (4)

$$\delta = \frac{\nu e^{\left(K\frac{u_\infty}{u^*} - KC - 2\Pi\right)}}{u^*}. \tag{10}$$

The first remarkable feature of the turbulent boundary layer is the universality of the near-wall ($y^+ \gtrsim 30$, $y^+/\delta^+ \ll 1$) behavior of Equation (4). Regardless of pressure gradient, wall roughness, or Reynolds number, the logarithmic dependence of u on y is observed.

The second remarkable feature is summarized by the results due to Klebanoff (1954) shown in Figure 3*a* which show that a sharp peak in the rate of production of turbulent energy (production $= -\langle u'v' \rangle \partial \bar{u}/\partial y$) occurs at the outer edge of the viscous sublayer. Measurements in pipe flow by Laufer (1954) show a similar effect. Integration over the thickness of the boundary layer leads to the result that the first 5% of the boundary layer contributes over half of the total production of turbulent energy. This important result was the primary motivation for the early work of Kline & Runstadler (1959) and later Kline et al (1967), and remains the primary motivation for much of the work on boundary-layer structure being carried on today.

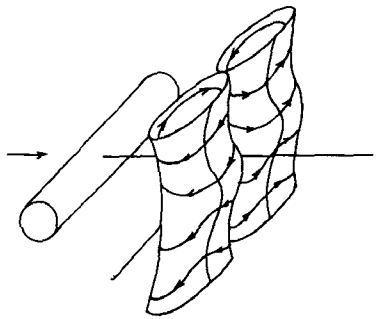

a

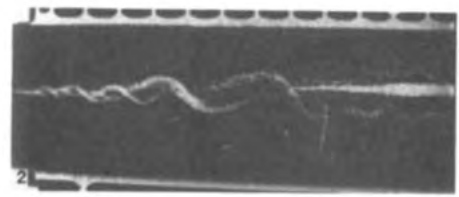

Figure 2 Eddy structure inferred from correlation measurements for several flows. (*a*) Cylinder wake by Payne & Lumley (1967); (*b*) Inclined double-roller structure for general shear flow from Townsend (1970); (*c*) Double-cone structure for wall flow from Townsend (1976).

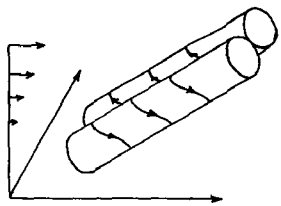

b

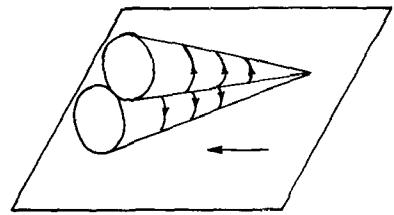

c

(b) *Methods of Approach*

Efforts to isolate coherent structure in the boundary layer have followed two basic lines of approach. The first approach uses various modified forms of the correlation method used by Townsend. The main disadvantage of this method in most of its various forms is that the details of the organized flow pattern in physical coordinates are not determined. The main advantage is that the coherent structure is represented within a well-defined mathematical framework that allows quantitative statements to be made about its statistical properties.

The second line of approach makes use of various methods of flow visualization to make direct observations of complex unsteady turbulent motions. Here, flow visualization is used in the broadest sense to include conventional methods using hydrogen bubble, dye, shadowgraph, and Schlieren techniques as well as nonconventional methods based on conditionally averaged velocity measurements tied together to form a picture of the flow pattern.

An extension of the Eulerian spatial-correlation method to a time-space correlation

$$R_{ij}(\mathbf{x}, \boldsymbol{\xi}, \tau) = \overline{u_i(\mathbf{x}, t) u_j(\mathbf{x}+\boldsymbol{\xi}, t+\tau)} \tag{11}$$

was used by Favre et al (1957) to retain phase information about the flow structure in a turbulent boundary layer. The spatial separation of probes plus the time delay for maximum correlation leads to information about the propagation velocity of the structure. In general, they were able to show that the large-scale streamwise velocity fluctuations are convected with the local mean speed. By placing two probes at different distances from the wall they found that a positive time delay of the signal from the probe nearest the wall was required for a maximum of the correlation coefficient, with the time delay increasing with increasing distance between the probes. From this they concluded that the convected turbulent structure was inclined to the wall. In addition, they found that the scale of the correlation of streamwise velocity fluctuations was much larger in the streamwise than in the cross-stream direction.

There is a subtle difference between the correlation method used by Townsend and that of Favre. Townsend uses spatial correlations to infer a physical picture of the large-eddy flow pattern, whereas the space-time correlation map itself often becomes the "physical" picture of the flow.

(c) Near-Wall Studies

Willmarth & Wooldridge (1962) used the space-time correlation to study pressure fluctuations at the wall under a thick turbulent boundary layer. Using two flush-mounted pressure sensors, they measured the correlation surface $R_{pp}(x, \tau)$ (x is in the streamwise direction) shown in Figure 4*a*. This figure shows two propagating maxima; one of these propagates against the flow, which they attribute to acoustic disturbances propagating upstream from the wind-tunnel diffuser. The main result is the maximum in R_{pp} leaning in the downstream direction which is associated with the propagation and decay of turbulent eddies. By filtering the measured R_{pp} in several frequency bands, they deduced roughly $u_c/u_\infty = 0.83$ for large pressure-producing eddies and $u_c/u_\infty = 0.69$ for small pressure-producing eddies. In contrast to the results of Favre et al they found that the spatial extent of the pressure correlation is approximately the same in directions parallel and transverse to the stream.

In a series of following papers (Willmarth & Wooldridge 1963, Tu & Willmarth 1966, see also the review by Willmarth 1975), this picture was extended and refined. Willmarth & Wooldridge (1963) introduced a scheme called the vector field of correlations in which a field of vectors with components R_{pu} and R_{pv} (p is wall pressure, u and v are velocity components at a fixed probe) is plotted in physical coordinates corresponding to the measuring points of the fixed velocity probe. The result

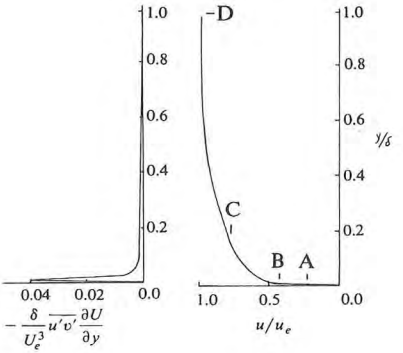

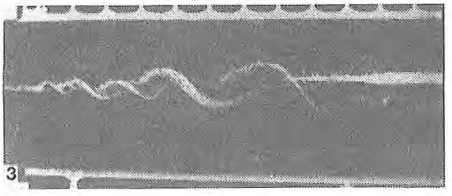

Figure 3 Mean behavior of a turbulent boundary layer. (*a*) Normalized turbulence-energy-production rate per unit volume (Klebanoff 1954); (*b*) Typical mean-velocity profile; (*c*) Sublayer streaks at $R_\delta = 9000$; (*d*) Sublayer streaks at $R_\delta = 26000$.

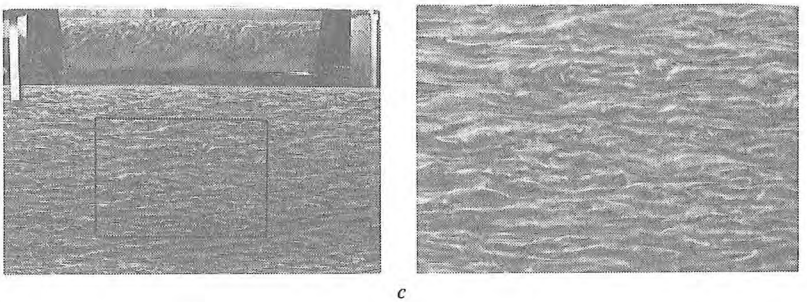

c

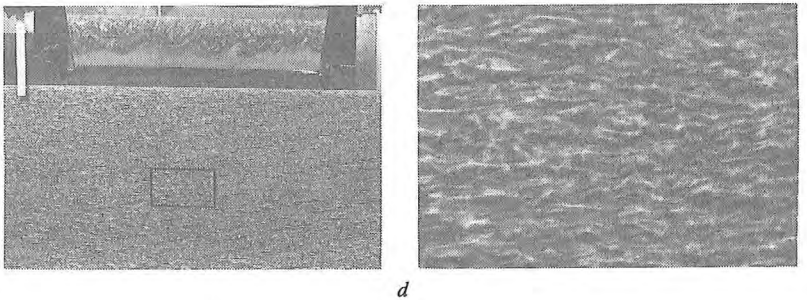

d

of such a correlation picture is shown in Figure 4*b*. Here the correlation map truly becomes a picture of the flow. In effect this picture represents a conditional average of the velocity field over an ensemble of flow disturbances and represents an early attempt to produce a picture of the velocity field associated with the organized structure in a turbulent boundary layer. Later work (Willmarth 1975) showed a strong correlation between streamwise velocity fluctuations and wall shear. In summary, three separate variables of the flow, the velocity field, wall

pressure, and wall shear were all found to be highly correlated over a significant portion of the boundary layer.

Beginning in the late 1950s, a series of experiments was begun at Stanford using flow visualization to study the turbulent boundary layer. This effort culminated in the work by Kline et al (1967). Several new features of the flow in the near-wall region of the turbulent boundary layer were revealed. The flow in a low-Reynolds-number turbulent boundary layer was visualized by a hydrogen-bubble wire placed parallel to, and at various distances above, the wall. They found that even when the wire was deep in the viscous sublayer at $y^+ = 2.7$ the bubbles did not follow straight trajectories as they moved slowly along the plate, but rather they accumulated into an alternating array of high- and low-speed regions called "streaks." They observed that the streaks interacted with the outer portions of the flow through a sequence of four events: gradual outflow, liftup, sudden oscillation, and breakup. To the sequence of three events from liftup to breakup they applied the term "bursting." In addition, they found that a favorable pressure gradient ($dP/dx < 0$) tended to reduce the rate of bursting and an unfavorable pressure gradient ($d\rho/dx > 0$) tended to increase the rate and intensity of bursting. It was conjectured that the bursting phenomenon plays a dominant role in the production of turbulent energy, that it dominates the transfer process between inner and outer regions of the boundary layer and in doing so plays an important role in determining the structure of the entire layer. Using combined dye and hydrogen-bubble visualization plus hot-wire measurements, Kline et al were able to estimate various scales of motion associated with the streaks and bursts. They deduced from visual data that the average spanwise streak spacing (i.e. the distance for one full wavelength) for a smooth wall in all pressure gradients was approximately $\lambda_z^+ = \lambda_z u^*/\nu = 100$. The sequence of events associated with bursting was as follows: Initially the streak of hydrogen bubbles drifts slowly downstream and outward from the wall. When the streak reaches $y^+ = 8-12$ it begins to oscillate. This oscillation amplifies and terminates in a very abrupt breakup in the region $10 < y^+ < 30$. After the breakup the streak of bubbles is contorted, stretched, and ejected outward along an identifiable trajectory. They observed that beyond $y^+ = 40$ the ejected fluid moves at about 80% of the mean velocity in the outer part of the boundary layer. Putting all the visual and quantitative information together they constructed the schematic picture of the streak breakup process shown in Figure 5*a*. The various stages in the bursting process are summarized in Figure 5*b*.

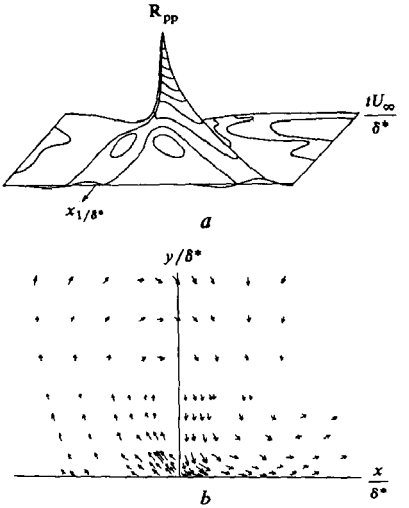

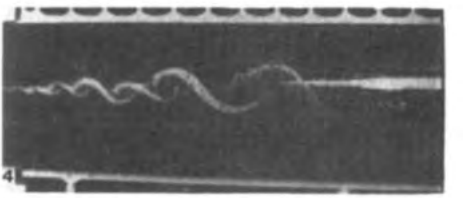

Figure 4 Turbulent boundary-layer structure based on space-time correlations by Willmarth & Wooldridge (1963). (*a*) Correlation between two pressure transducers mounted flush with the wall; (*b*) Vector field of pressure-velocity correlations, magnitude of the vector at any point is $(R_{pu}^2+R_{pv}^2)^{1/2}$, direction of the vector is $\tan^{-1}(R_{pv}/R_{pu})$.

Corino & Brodkey (1969) observed what they called ejections near the wall in fully developed high-Reynolds-number pipe flow. In contrast to Kline et al, they viewed the sublayer ($y^+<5$) as essentially passive with the ejections originating in a zone away from the wall between $y^+=5$ and $y^+=15$. It was noticed that the ejection always ended with an action called a sweep, which consisted of axial movement of upstream fluid sweeping out fluid from the previous ejection event. They examined the effect of Reynolds number on the frequency of the ejection process over a range from 2300 (laminar flow) to 50,000 and in general found that the number and intensity of events increased with increasing Reynolds number. Corino & Brodkey estimated that the ejections accounted for approximately 70% of the Reynolds stress measured by Laufer (1954).

These results were confirmed by Kim et al (1971) who showed that virtually all of the net production of turbulent energy in the range $0<y^+<100$ occurs during bursts.

Willmarth & Lu (1972) studied the instantaneous $u'v'$ product near the wall and found very large values during bursting with rare events reaching $u'v'\sim 60\langle u'v'\rangle$ at $y^+=30.5$. They also found that large contributions to the Reynolds stress occurred during the sweep phase observed by Corino & Brodkey. A similar observation was also made by Grass (1971). Prior to this, most of the contributions to the Reynolds stress were assumed to occur during the outflow of low-speed fluid.

Taken together, these initial observations constitute a significant step, which has provided the inspiration for much of the work on turbulent

boundary layers that has followed. They illuminate an important link between a quasi-deterministic, repeatable unsteady motion and the production and maintenance of mean turbulent transport.

In the initial studies of bursting the process was viewed as an essentially wall-bounded phenomenon with scales of motion determined from wall parameters u^* and ν. Thus it came as something of a shock when Rao et al (1971), after examining data over a fairly wide range of Reynolds number ($600 < R_\theta < 9000$),[3] showed that even in the wall layer the mean burst period scales with outer (u_∞, δ) rather than inner (u^*, ν) variables with the mean dimensionless time between bursts given by

$$\frac{u_\infty T}{\delta} \approx 6. \tag{12}$$

Moreover, they found that the mean burst rate did not vary greatly with distance from the wall. Rao et al suggested that such bursts may be a general feature of *all* turbulent flows. They visualized large outer eddies scouring the slow-moving inner layer releasing bursts of turbulent energy by creating regions of intense shear in the inner layer by triggering local instabilities. The inner layer is seen as neither passive nor solely responsible for energy production, but as strongly interacting with the outer layer. They also suggest a mixed scaling with inner variables for the spanwise spatial scale and outer variables for the time between bursts which leads to $u_\infty u^*/F\delta^*\nu$ (where δ^* is displacement thickness and F is the burst rate per unit span) as a quantity that is practically independent of Reynolds number. Aside from brief discussions in Kline et al and Rao et al, the remaining literature on this subject takes relatively little notice of the need for information on the scaling parameters for the spanwise spacing between bursts.

In an excellent and very extensive study, Grass (1971) used hydrogen-bubble data corrected for the lag effect due to the bubble-wire wake to measure structural features of turbulent flow over smooth, transitionally rough, and fully rough walls ($u^*k/\nu = 0.0$, 20.7, 84.7 where k is the roughness height). He found that ejections and inrushes were present irrespective of the surface roughness. Grass suggests a universal ejection type of momentum-transport mechanism which extends across a major portion of the boundary-layer thickness. The mechanism is visualized as jets of low-momentum fluid ejected from the boundary region and randomly distributed with respect to position and time. He suggests further that the general ejection process is a common feature of the flow

[3]The range has since been extended by Narayanan & Marvin (1978) to $600 < R_\theta < 35{,}000$.

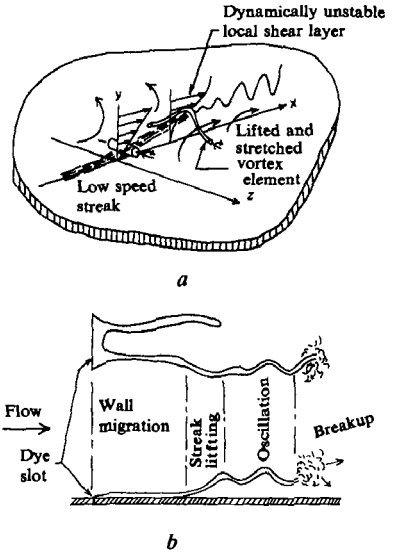

Figure 5 Schematic views of near-wall turbulent boundary-layer structure based on direct observations. (*a*) Mechanics of streak breakup by Kline et al (1967), (*b*) Sequence of events in (*a*) by Kline (1978).

structure irrespective of boundary-roughness conditions. This is an important conjecture that raises some question regarding the precise role of sublayer streaks in the bursting process. The wall flow of a fully rough-wall boundary layer must be substantially different from that of a smooth-wall boundary layer. Yet the basic structure of the organized motion appears to be largely unchanged.

More recently, Blackwelder & Eckelmann (1979) have made a rather detailed study of the structure of wall streaks using heated wall elements to infer streamwise and spanwise vorticity at the wall (Figures 6*a* and *b*). They find the strength of streamwise vortices to be about one order of magnitude less than the mean spanwise vorticity. They identify the low-speed streak observed by Kline et al and others as the accumulation region between streamwise vortices where the vertical component of the secondary motion is directed away from the wall. They find the streamwise length of the vortices to be $\Delta x^+ \sim 1000$.

(d) Outer-Flow Studies

As evidence for organized structure near the wall accumulated, attention began to focus on the flow in the outer part of the layer and the possible connection or interaction which may exist between the outer and wall layer.[4] Kovasznay et al used conditionally averaged space-time

[4]As a general rule, the term "wall layer" refers to $0 < y^+ < 100$, which includes the viscous sublayer and a portion of the logarithmic region. The term "outer layer" refers to all the rest.

autocorrelations of several flow variables to draw a three-dimensional correlation map of the outer structure (Figure 7). They observed that the vorticity appeared to exhibit a discontinuity across the turbulent interface of the bulge whereas the velocity was continuous. In addition, they noticed that there was a considerable difference between the upstream-facing (back) and downstream-facing (front) portions of turbulent humps in the outer flow. They suggest, almost in passing, that if the flow were viewed in a coordinate system moving with the average convection velocity of the interface, fluid would appear to arrive at a stagnation point on the back of a bulge located at about $y/\delta = 0.8$. This brief remark represents a most important observation which forms part of a common thread that runs through much of the recent literature on organized structure in turbulent flow; that it is the upstream-facing portion of the turbulent-nonturbulent interface that is most active, and that this activity is associated with a saddle-point flow in a convected frame of reference. A wide variety of flows, not just turbulent boundary layers, seem to exhibit this property. Observations of intense turbulent activity along upstream-facing interfaces may be found in Wygnanski & Champagne (1973; the turbulent slug in pipe flow), Falco (1977; turbulent boundary layer), Brown & Thomas (1977; turbulent boundary layer), Wygnanski et al (1976; turbulent spot), Cantwell et al (1978; turbulent spot), Gad-el-Hak & Blackwelder (1979; turbulent spot), and Cantwell & Coles (1980; cylinder near wake).

Kovasznay et al found that the individual bulges in the outer flow are correlated over 3δ in the streamwise direction and δ in the spanwise direction. They conjecture that the bulges in the interface become passive and that only the birth of new ejected lumps (presumably from the wall) is the mechanism that maintains the Reynolds stress of the outer layer. They speculate that the bursts observed by Kline et al (1967) near the wall are responsible for the large-scale motion in the outer flow that they observe. They also conjecture that the large-scale wall-pressure fluctuation pattern may be caused by the same mechanism.

Blackwelder & Kovasznay (1972) extended the earlier work with measurements closer to the wall. They found that intense motions in the wall region remained strongly correlated out to $y/\delta \approx 0.5$ confirming other observations that the disturbance associated with bursting extends across the entire layer.

In a pair of papers, Offen & Kline (1974, 1975) attempted to draw a kinematical description of the relationship between the inner and outer flow. They posed a causal relationship for the interaction between bursts and the flow in the logarithmic region that produces sweeps

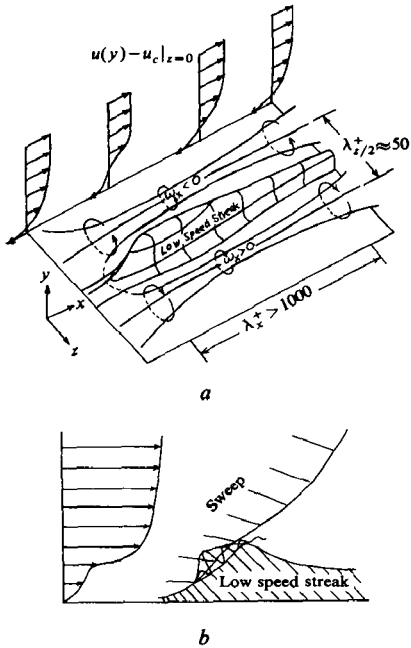

Figure 6 Model of near-wall turbulent boundary-layer structure from Blackwelder (1978). (*a*) Counter-rotating streamwise vortices with the resulting low-speed streak; (*b*) Localized shear-layer instability between an incoming sweep and low-speed streak.

which, in turn, influence the generation of bursts farther downstream. Inspired partially by observations of vortex interactions in the plane mixing layer, they advanced the hypothesis that the bulges in the superlayer may be the consequence of vortex pairing between the vortices associated with two to four bursts.

Brown & Thomas (1977) correlated wall shear with velocity across the layer. They observed that the wall shear has a slowly varying part and a high-frequency part and that the two appear to be coupled. They established a line of maximum correlation which lay at an angle of 18° to the wall in the downstream direction and hypothesized that this was due to some organized structure at an oblique angle to the wall which produces a characteristic response in wall shear as it moves along the plate at about 0.8 u_∞. They also observed a sharp step in the velocity which occurs at the trailing interface of the outer bulge. Falco (1977) combined visual and hot-wire observations in the outer layer. He also noticed considerable activity on the trailing interface of the outer bulge which he associated with Reynolds-stress-producing motions due to small-scale eddies in the outer layer with length scales on the order of 100 to 200 ν/u^*. Brown & Thomas, Falco, and Blackwelder & Kovasznay draw very similar sketches of the organized structure (Figures 8*a*, *b*, and *c*).

In an extensive visual study, Smith (1978) used a moving frame of reference to study the interaction between inner and outer layers in a turbulent boundary layer at Reynolds numbers somewhat higher than the range studied by Falco. He observes the burst sequence to be related to the passage of a large-scale motion with a generally transverse rotation similar to observations by Nychas et al (1973). The large-scale motion is described as an agglomeration of smaller-scale vortical structures of varying sizes, strengths, orientations, and coherency with an overall spanwise rotation. Velocities of different structures within the large-scale motion varied from 0.7 u_∞ to 0.95 u_∞ with the center of rotation moving at about 0.8 u_∞. In some of the observations of the interaction of wall-region fluid with the outer flow, free-shear-layer type vortical structures were observed to form in a region between $y^+ = 10$ and 40. He argues that the formation of these spanwise wavelike motions is a key mechanism in the entrainment process of the low-speed, wall-region fluid into the higher-speed sweep fluid and thus is a source of the high-Reynolds-stress production in the wall region during the bursting process.

Head & Bandyopadhyay (1978) used flow visualization and hot-wire measurements to draw quite a different picture of the turbulent boundary layer (Figure 9*a*). They make the point that Reynolds-number effects on the detailed boundary-layer structure are likely to be important and that experiments at $Re_\theta < 1000$ (which covers about two-thirds of the literature on this subject) may give results that are quite unrepresentative of those at really high Reynolds numbers. They suggest that for values of Re_θ in the range 1000–7000 the most characteristic feature of the boundary layer is not the existence of large-scale coherent motions, but of structures formed by the random amalgamation of features that are small in the streamwise direction but highly elongated along lines at about 40° to the surface. It is inferred that these represent hairpin vortices similar to the horseshoe vortices postulated by Theodorsen (1955). They suggest that the Reynolds-stress-producing outer eddies of Falco are in fact the tips of the hairpin vortices. This model has some features in common with some recent computations by Leonard (1979) of three-dimensional vortex motions in a developing turbulent spot (Figure 9*b*). Here, initially transverse vortex lines near a wall are perturbed and the perturbation is allowed to grow. Eventually a large-amplitude motion is observed in which the (now wavy) array of vortex lines assumes a shape similar to a family of Theodorsen vortices with their heads pointed downstream at an inclined angle to the plate. More recently, Perry et al (1980) have proposed a model of near-wall boundary-layer structure based on strings of Λ-shaped vortices similar

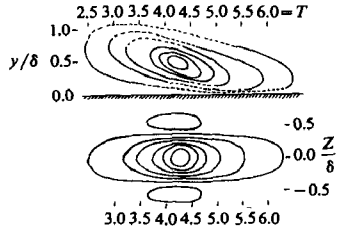

a

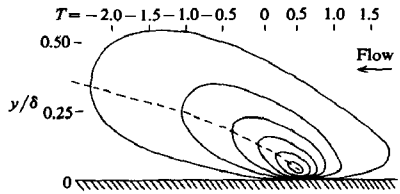

b

Figure 7 Turbulent boundary-layer structure based on space-time correlations between the velocity at a fixed probe and the velocity at a probe that is positioned at various points in the flow. (*a*) Fixed probe at $y/\delta = 0.5$ from Kovasznay et al (1970); (*b*) Fixed probe at y/δ 0.03 from Blackwelder & Kovasznay (1972).

to those observed in a visual study of boundary-layer turbulence by Hama & Nutant (1963). Their model reproduces a number of the mean features of wall turbulence including the logarithmic velocity profile.

All of the investigations discussed thus far have involved observations in naturally occurring turbulent boundary layers. Several additional investigations should also be noted. Zilberman et al (1977) generated turbulent spots and allowed them to pass into a turbulent boundary layer that was tripped by a spanwise array of spheres. They were able to track the perturbation associated with the spot for approximately 70 turbulent-boundary-layer thicknesses in the streamwise direction. The convection speed of the disturbance was 0.9 u_∞ and the main features of the spot structure imbedded in the boundary layer were in general agreement with other observations of the outer large structure.

Part of the difficulty in measuring the organized motion lies in the fact that it is extremely difficult to isolate and average. An interesting solution to this dilemma was proposed by Coles & Barker (1975). They created a synthetic boundary layer in water by using a series of controlled disturbances near the leading edge of a flat plate. These produced systematic moving patterns of turbulent spots in a laminar flow which, when averaged, gave a turbulent boundary layer with a standard mean-velocity profile. The idea here is to create a flow that simulates the naturally occurring flow but is much easier to study. This work has been continued in an air boundary layer by Savas (1979) who made extensive measurements of intermittency in the outer part of the layer. He found that the celerity of outer large eddies was 0.88. Savas

observed an interaction phenomenon he called "eddy transposition." This involves the appearance and rapid growth of regions of new turbulence to the rear of the original spots and in the gaps between them. The original spots then decay and disappear. During the transposition process the number of large eddies is twice the normal value and these eddies form a honeycomb pattern of hexagons with empty centers. When transposition is complete, the original hexagonal pattern is restored with a substantial phase shift. Savas suggests that by fitting spots together in a close-packed hexagonal pattern spaced 2.5δ in the spanwise direction and about 8δ in the streamwise direction, one can create an optimal synthetic boundary layer.

(e) Other Wall-Bounded Flows

A number of the works discussed in the last section have involved studies in fully developed pipe flow. However, no discussion of coherent motion in turbulent flow would be complete without some discussion of the remarkably complex transition in pipe flow. Motivated partially by the observations of Lindgren (1969), Wygnanski & Champagne (1973) undertook an extensive study of transition in a pipe over a Reynolds-number range from 2000 to 50,000. For smooth or only slightly disturbed inlets, transition occurs as a result of instabilities in the developing boundary layer long before the flow becomes fully developed in the pipe. This type of transition gives rise to turbulent slugs, which may occur at any Reynolds number greater than 3200. They occupy the entire cross-section of the pipe (Figure 10*a*) and grow in length as they proceed downstream. Although the lengths of individual slugs vary, an upper limit is of the order of the length of the pipe. The structure of the flow in the interior of a slug is identical to that in a fully developed turbulent pipe flow. Near the front and rear interfaces where the mean motion changes from a laminar to a turbulent state, the velocity profiles develop inflections. The total turbulence intensity near the interfaces is generally four to seven times higher than in the interior of the slug and may reach 15% of the velocity at the center of the pipe. The maxima in the Reynolds stresses occur at approximately the same location as the inflection points in the velocity profile. Slugs were never observed while the velocity profile was close to parabolic. The implication of this is that stability calculations in the developing region of the pipe are more relevant to the natural process of transition in a pipe than the analyses that are solely concerned with the stability of Poiseuille flow. Wygnanski & Champagne found a second type of intermittently turbulent flow which involved "puffs" of mixed laminar and turbulent flow in the fully developed portion of the pipe for $2000 < \mathrm{Re} < 2700$. Puffs are formed when a large disturbance is introduced at the inlet. While slugs are

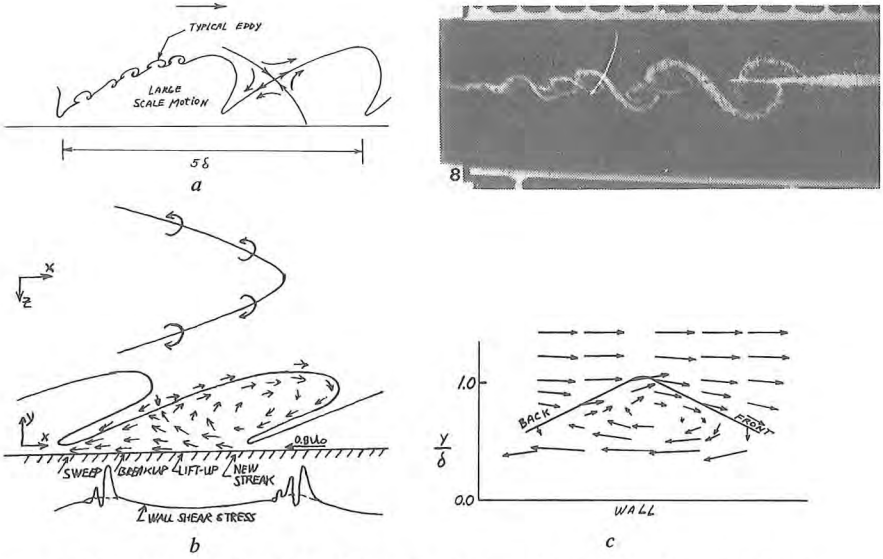

Figure 8 Three conceptual models of the outer structure of a turbulent boundary layer. Each figure is referenced to an observer who moves at 0.8 u_∞. (*a*) A composite of several figures from Falco (1977); (*b*) Outer flow plus wall shear from Brown & Thomas (1977); (*c*) From Blackwelder & Kovasznay (1972).

associated with transition from laminar to turbulent flow in the wall layer of the inlet flow, puffs apparently correspond to an incomplete relaminarization process. Occasionally puffs were observed to split and/or decay. Puffs can only be seen at $2000 \leqslant \mathrm{Re} \leqslant 2700$, whereas slugs occur at any $\mathrm{Re} > 3200$.

Wygnanski et al (1976) carried out a fairly extensive study of the puff. They were able to produce turbulent puffs that would maintain themselves indefinitely at Reynolds numbers around 2200. Nonequilibrium puffs at Reynolds numbers away from this value tend to grow and split or decay. The various regimes are as follows:

$\mathrm{Re} \leqslant 2200$	Puffs diminish with x.
$2200 \leqslant \mathrm{Re} \leqslant 2300$	A single disturbance at the inlet gives rise to a single puff. No splitting is observed. The puff appears to be in equilibrium.
$2300 \leqslant \mathrm{Re} \leqslant 2600$	Puffs grow with x. As Re increases, the number of puffs per disturbance increases reaching a maximum of four at $\mathrm{Re} = 2600$.
$2600 \leqslant \mathrm{Re} \leqslant 2800$	A further increase of Re decreases the number of puffs until at $\mathrm{Re} \approx 2800$ a single slug of turbulence is observed.
$\mathrm{Re} \geqslant 3200$	Only slugs are observed.

Wygnanski et al (1976) made measurements of the equilibrium puff at Re=2220. A streamline picture of the puff in moving coordinates is shown in Figure 10*b*. In this frame of reference, the flow consists of two large flattened ring vortices which rotate in the same direction along with a small eddy in the vicinity of the rearward interface. The turbulent intensity in the puff increases gradually towards the rear of the puff and attains a maximum at the trailing edge. Near the leading edge of the puff there is no clear interface between laminar and turbulent flow, in contrast to the turbulent slug which is bounded by two well-defined interfaces spanning the entire cross section of the pipe.

Another curious, highly organized, wall-bounded flow is the spiral turbulence between two counter-rotating cylinders studied by Coles & Van Atta (1967). Under certain conditions the flow between two concentric, counter-rotating, cylinders consists of helical bands of alternating laminar and turbulent flow. The band of turbulence rotates at a speed roughly halfway between the speed of the inner and outer cylinders (Figure 10*c*). Fluid enters the turbulence at a severe angle, but leaves at a grazing angle so that the rate of detrainment of fluid passing from a turbulent to a laminar state is actually very low. In fact, the shape of the upstream-facing interface appears to be controlled primarily by the process of viscous decay. A similar observation was made by Wygnanski & Champagne in the turbulent slug in pipe flow. They found that a unique relationship existed between the velocity of the fluid and the velocity of the upstream-facing interface such that sudden relaminarization of turbulent fluid is prevented.

Another wall-bounded flow that has received considerable attention is the turbulent spot first studied by Emmons (1951) and Mitchner (1954). Shortly after these initial observations, Schubauer & Klebanoff (1955) defined celerities (0.55–0.9) for the upstream and downstream interfaces of the spot. Elder (1960) looked at the merging of spots and found a strongly nonlinear interaction in which one spot merges with another with very little loss of identity. Coles & Barker (1975) and Wygnanski et al (1976) made detailed measurements of the streamline pattern of an average spot. Both investigations concluded that the ensemble-averaged spot was essentially a single large horseshoe vortex superimposed on small-scale motions, which average out in the mean. The structure is not unlike a Theodorsen vortex, but larger. The extensive detail of the pictures drawn by Wygnanski et al of the puff and spot (Figures 10*b* and 11*a*) and Coles & Barker of the spot represent a significant advance over earlier attempts to visualize organized motion in turbulence. They also represent something of a retrenchment from the complexity of the turbulent boundary layer to flows where the

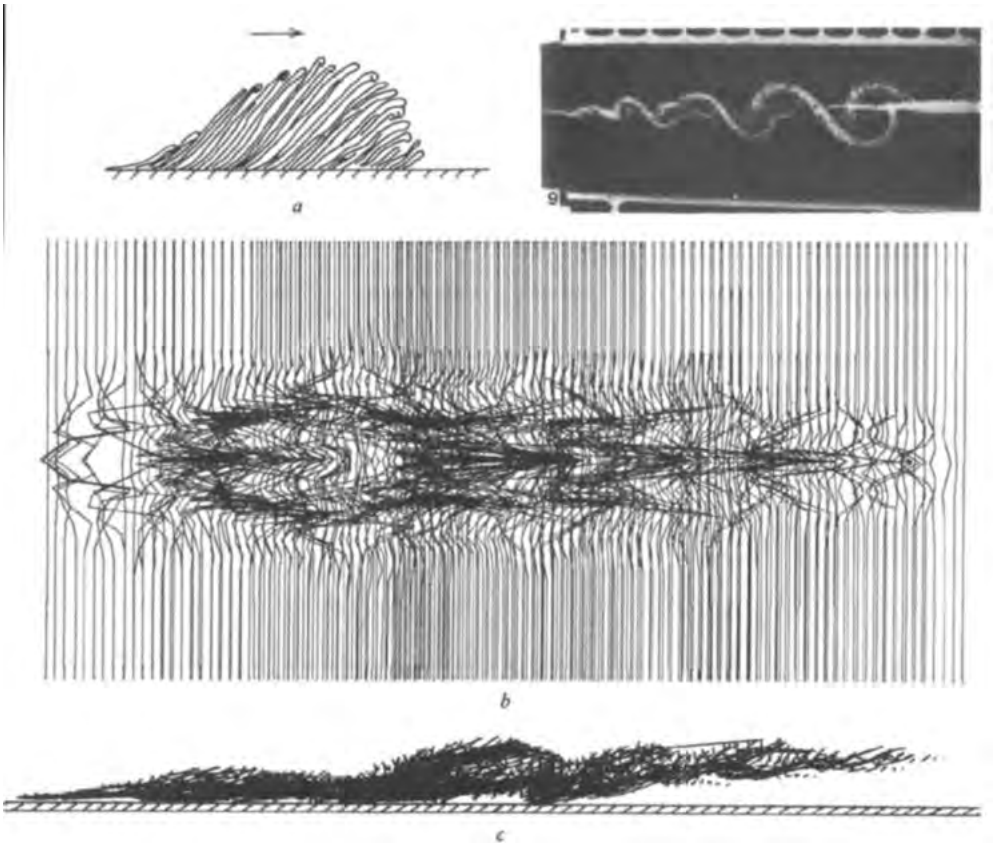

Figure 9 (*a*) A conceptual model of turbulent boundary-layer structure based on highly elongated horseshoe vortices by Head & Bandyopadhyay (1978); (*b*) and (*c*) Vortex lines in a developing turbulent spot computed by Leonard (1979).

organized motion is much easier to isolate and identify. As for most of the major features of the spot, both investigations were in generally good agreement. There was, however, one major area of disagreement related to the celerity of the most energetic part of the motion. Space-time correlations near the wall led Wygnanski et al to a celerity of 0.65 u_∞. Coles & Barker observed a conspicuous minimum in the streamwise velocity in the outer part of the spot. By timing the arrival of this minimum at several stations downstream of the spot origin they deduced a celerity of 0.83 u_∞.

Cantwell et al (1978) carried out measurements on the plane of symmetry of the spot and made use of the approximately conical behavior of the spot to collapse their velocity data using similarity variables $\xi = x/u_\infty t$, $\eta = y/u_\infty t$ and $u/u_\infty = U(\xi, \eta)$, $v/u_\infty = V(\xi, \eta)$. In

these coordinates, the equations for unsteady particle paths reduce to an autonomous system which can be integrated graphically by simply plotting isoclines. The result of this process is a diagram (Figure 11*c*) showing how the spot entrains free stream fluid. A useful property of the entrainment diagram is that it is invariant for all uniformly moving observers. As a result, structural features of the flow are brought out in a simple and invariant way without reference to the speed of a moving observer. The entrainment diagram for the spot includes four critical points, two saddles and two stable foci. The outer focus moves at 0.78 u_∞ and is probably responsible for the velocity minimum observed by Coles & Barker. The inner focus moves at 0.65 u_∞, the same speed deduced from the maximum space-time correlation measurements of Wygnanski et al.

More recently, Wygnanski et al (1979) have found that the laminar relaxation region following the spot is occupied by Tollmien-Schlichting instability waves induced by the fluctuating motions near the outer wings of the spot. They suggest that spot growth is controlled by the formation of new spots due to the breakdown of the trailing Tollmien-Schlichting waves.

(f) Summary of the Flow Structure

We have seen a procession of different views of turbulent-boundary-layer structure deduced using a variety of methods. Each method has its own special advantages and disadvantages. The correlation approach leads to well-defined pictures which contain substantial amounts of quantitative statistical information. However, it tends to be unphysical and yields little information about the detailed structure of the flow. The direct approach using flow visualization is more physical but leads to conflicting results which are often difficult to interpret and organize. The problem here has often been compared to the fable about the five blind men and the elephant. Each man explores a small part of the animal and then makes conclusions about the nature of the whole beast. The fable points out the limits of human observation compared to the totality of facts required to make a correct conclusion.

Any attempt to summarize various data for organized structure in the turbulent boundary layer runs smack into a maze of ambiguous labels and conflicting definitions. Most observed quantities exhibit wide variation about a poorly defined mean. As a result common denominators are rare. Nevertheless, certain properties of the organized structure are beginning to be established.

There appear to be four main constituents of the organized structure. Nearest the wall is a fluctuating array of streamwise counter-rotating

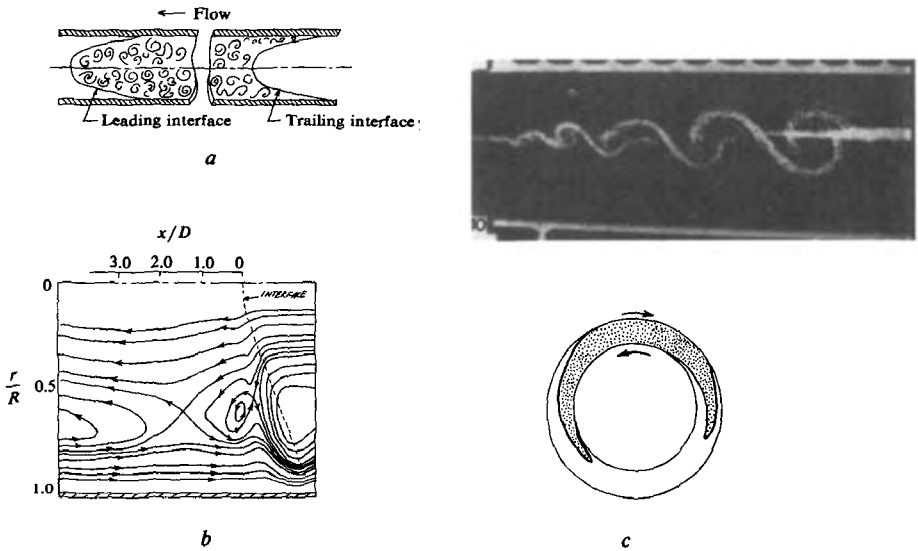

Figure 10 Organized motion in pipe flow. (*a*) Schematic of a turbulent slug from Wygnanski & Champagne (1973); (*b*) Ensemble-averaged streamline patterns in a turbulent puff from Wygnanski et al (1976); spiral turbulence (*c*) from Coles & Van Atta (1967).

vortices. See Figures 3*c* and *d*. The vortices densely cover all parts of the smooth wall. Slightly above the streamwise vortices but still quite close to the wall is a layer that is regularly battered by bursts that involve very intense small-scale motions of energetic fluid. The outer layer is also occupied by intense small-scale motions. These are found primarily on the upstream-facing portions of the turbulent-nonturbulent interface; the backs of the bulges in the outer part of the layer. The outer small-scale motions are part of an overall transverse rotation with a scale comparable to the thickness of the layer. The various components, along with some notation, are summarized schematically in Figure 12. These components and fairly crude estimates of their scale, position, celerity, and lifetime are discussed below.

1. λ_x—Length of sublayer structure in the streamwise direction (Blackwelder 1978, Blackwelder & Eckelmann 1979, Praturi & Brodkey 1978). Observations vary from $\lambda_x = 100\ \nu/u^*$ to $\lambda_x = 2000\ \nu/u^*$ with $1000\ \nu/u^*$ as a best value. An issue here, which may account for some of the variation, is the distinction between sublayer streaks and sublayer longitudinal vortices. The consensus of data seems to be that streaks are the product of an accumulation process in regions that lie between streamwise vortices where there is an upwelling of fluid in the secondary motion (motion in a plane normal to the direction of flow). The

longitudinal scale of streaks might be quite different from the longitudinal scale of the secondary vortex motions that produce the accumulation. The exact form of the secondary streamline pattern associated with sublayer vortices, and how this pattern is matched to the more random secondary motions in the outer flow, is at present unclear.

2. λ_y—Vertical half scale of sublayer structure based on the distance from the wall to roughly the center of a streamwise vortex (Kline et al 1967, Bakewell & Lumley 1967, Blackwelder & Eckelmann 1979, Kovasznay et al 1970). Observations vary from $\lambda_y = 10\ \nu/u^*$ to $\lambda_y = 25\ \nu/u^*$ with $15\ \nu/u^*$ about average. Note that $y^+ = 30$ is about the vertical distance at which the law of the wall (Equation 4) begins to be valid.

3. λ_z—Spanwise (full wavelength) scale of sublayer structure (Kline et al 1967, Bakewell & Lumley 1967, Kim et al 1971, Grass 1971, Smith 1978, Praturi & Brodkey 1978, Cantwell et al 1978, Gupta et al 1971, Oldaker & Tiederman 1977, Hanratty et al 1977, Lee et al 1974, Willmarth & Yang 1970). This is probably the most universally agreed upon quantity in turbulent boundary-layer structure. The accepted mean value is $\lambda_z = 100\ \nu/u^*$. The statistics of this quantity are somewhat skewed, with the most probable value around $80\ \nu/u^*$. Some observations (Gupta et al 1971) indicate a possible dependence of $\lambda_z u^*/\nu$ on Reynolds number.

4. b_x, b_y, and b_z—Length scales of energetic near-wall eddies (Corino & Brodkey 1969, Dinkelacker et al 1977, Smith 1978, Sabot et al 1977). Here the correspondence between observations by different investigators becomes very difficult to pin down. However, it appears that in a region between $y^+ = 5$ and 40 very energetic parcels of fluid are observed to form through some mechanism of instability, which has yet to be fully identified. Most often the mechanism is described in terms of a fast inviscid oscillatory instability arising from a slowly varying instantaneous inflection point in the velocity profile (Figure 6*b*). Assigning scales to the parcel of fluid that participates in this process is very uncertain; however, typical estimates range from $20\ \nu/u^*$ to $40\ \nu/u^*$ for b_x and from $15\ \nu/u^*$ to $20\ \nu/u^*$ for b_y. There is essentially no information on b_z although the observations of Smith (1978) suggest that b_z may be several times b_x or b_y. Measurements based on wall pressure of the streamwise extent of energetic small-scale motions lead to somewhat larger estimates for b_x on the order of $60\ \nu/u^*$ to $100\ \nu/u^*$.

5. X_b—The persistence distance of energetic near-wall eddies (Dinkelacker et al 1977, and Praturi & Brodkey 1978). Values of X_b between 0.5δ and 1.5δ are suggested although the evidence is very sparse with wall-pressure measurements indicating the larger value.

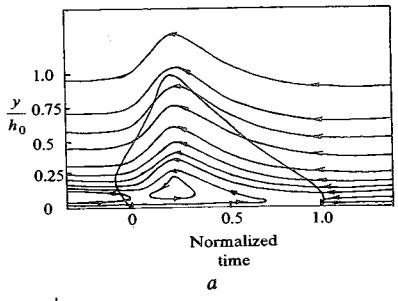

a

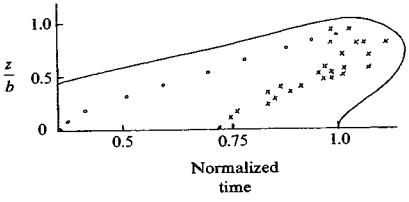

b

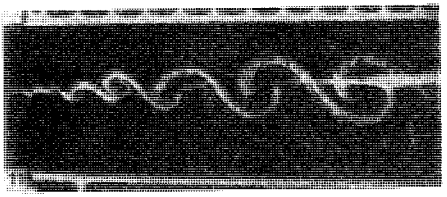

Figure 11 Organized motion in the turbulent spot. (*a*) Streamlines referenced to a moving observer; (*b*) Points of maximum space-time correlation from Wygnanski et al (1976); (*c*) Pathlines on the plane of symmetry from Cantwell et al (1978).

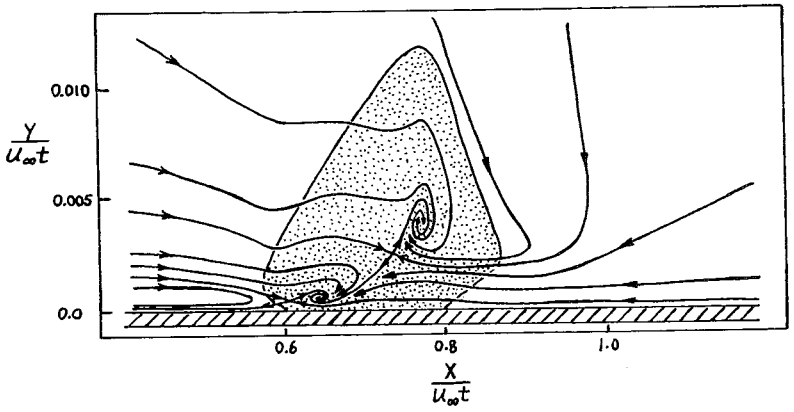

c

6. C_b—The celerity of energetic near-wall eddies (Kline et al 1967, Dinkelacker et al 1977, Brown & Thomas 1977, Cantwell et al 1978, Willmarth & Wooldridge 1962, Wygnanski & Champagne 1973). Most data indicate a value of C_b around $0.65\,u_\infty \pm 0.05\,u_\infty$. Wall-pressure data (Dinkelacker et al, 1977) indicate a much lower value around $0.2\,u_\infty$.

7. l_x, l_y, l_z—Length scales of energetic outer-flow eddies (Falco 1977, Zilberman et al 1977, Smith 1978). Called "typical eddies" by Falco, these outer-flow motions appear to be slightly flattened mushroom vortices with l_x on the order of 200 ν/u^* and l_y on the order of 100 ν/u^*. There is no specific information on l_z; however, a value between

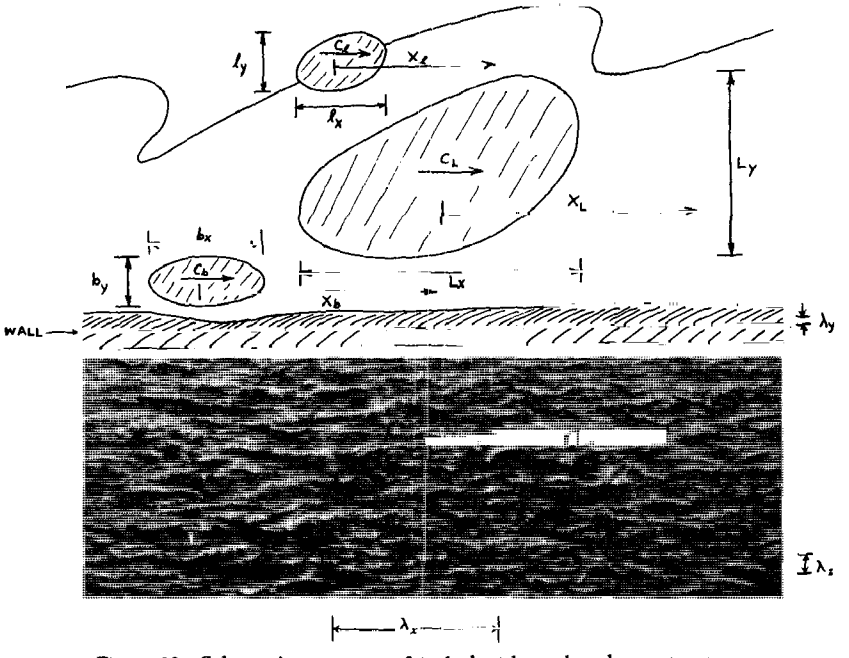

Figure 12 Schematic summary of turbulent boundary-layer structure.

100 and 200 ν/u^* would be expected. Falco suggests that the typical eddies scale with the Taylor microscale and that they account for a significant fraction of the Reynolds stress in the outer flow. This is contrary to the commonly held belief that the Reynolds stresses are produced primarily by the largest eddies in the flow. The evidence thus far is relatively sparse and more measurements are needed over a wide Reynolds-number range to confirm these observations.

8. X_l—Persistence distance of energetic outer-flow eddies. These eddies appear to travel approximately five times their own streamwise length or about 1000 ν/u^* before losing their identity.

9. C_l—Celerity of energetic outer-flow eddies (Kovasznay et al 1970, Smith 1978, and Savas 1979). Typical values between 0.8 u_∞ and 0.9 u_∞ are observed.

10. L_x, L_y, L_z—Length scales of the large-scale motion in the outer flow (Kovasznay 1970, Dinkelacker et al 1977, Brown & Thomas 1977, Falco 1977, Zilberman et al 1977, Smith 1978, Head & Bandyopadhyay 1978, Praturi & Brodkey 1978, Willmarth & Wooldridge 1962). Most observations give a value for L_x between δ and 2δ at a height of about 0.8δ above the surface. L_x inferred from wall-pressure data is somewhat smaller with typical values between 0.5δ and δ. At 0.8δ above the surface, the width L_z of the outer large eddy appears to be between 0.5δ

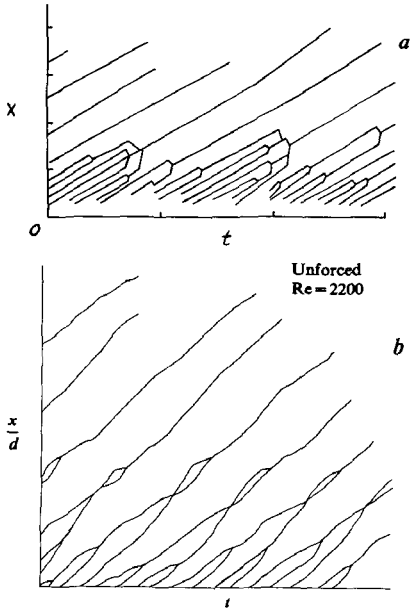

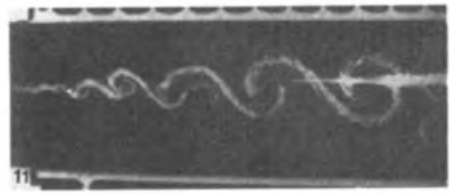

Figure 13 Vortex trajectories. (*a*) In a plane mixing layer from Brown & Roshko (1974); (*b*) In the axysymmetric mixing layer in the initial region of a jet from Bouchard & Reynolds (1978).

and δ with the eddy centers spaced about 2.0 to 3.0δ apart in the spanwise direction.

11. X_L—Persistence distance of the large-scale motion in the outer flow (Kovasznay et al 1970, Dinkelacker et al 1977). Typical values are about 1.6δ and 2δ at a height of about 0.8δ above the plate.

12. C_L—Celerity of the large-scale motion in the outer flow (Kovasznay et al 1970, Dinkelacker et al 1977, Brown & Thomas 1977, Zilberman et al 1977, Smith 1978, Savas 1979, Cantwell et al 1978, Sabot et al 1977, Zakkay et al 1978, Willmarth & Wooldridge 1962, Coles & Barker 1975). A variety of measurements indicate a value between 0.8 and 0.9 u_∞ at a height of about 0.8δ. Some wall-pressure data indicate a somewhat lower value.

13. T_B—Period between bursts (Kline et al 1967, Kim et al 1971, Rao et al 1971, Kovasznay et al 1970, Brown & Thomas 1977, Falco 1977, Narayanan & Marvin 1978, Smith 1978, Savas 1979, Sabot et al 1977, Zakkay et al 1978). This is one of the more studied variables in turbulent boundary-layer structure. Early observations scaled T_B with wall variables. Now it appears to be fairly well established that T_B scales with outer variables and the generally accepted number is $T_B u_\infty/\delta \simeq 6$; however, there is a considerable amount of scatter about this value with a range from 2.5 to 10. It is also found that T_B varies only slightly across the layer implying, in agreement with other observations, that the occurrence of a burst affects the entire layer.

14. β—Angle of maximum correlation (Corino & Brodkey 1969, Brown & Thomas 1977, Head & Bandyopadhyay 1978). Measurements correlating wall shear and streamwise velocity give $\beta = 18°$. Other observations of a characteristic lean angle for the large structure range from 8° to 40°.

15. $u'v'_{max}$—Maximum measured instantaneous $u'v'$ (Lu & Willmarth 1973, Falco 1977, Nychas et al 1973). In the outer portion of the flow ($y/\delta = 0.8$), instantaneous values of $u'v'$ exceeding ten times the local mean have been observed. Near the wall ($y^+ \sim 30$) values of $u'v'$ as large as 60 times the local mean have been observed.

16. $C_{pw_{max}}$—Maximum change in wall-pressure coefficient (based on free-stream velocity) during the passage of the organized motion (Dinkelacker et al 1977, Savas 1979, Cantwell et al 1978). Peak-to-peak variations on the order of 0.035 to 0.050 are observed.

17. w'_x—Root-mean-square streamwise vorticity fluctuations near the wall (Willmarth & Bogar 1977, Hanratty et al 1977). Typical values around one tenth the mean vorticity in the spanwise direction are observed.

18. $u^{+\prime}_{max}$—Maximum value of $\langle u'^2 \rangle^{1/2}/u^*$ (Coles 1978). This maximum occurs at about $y^+ = 15$. In an extensive survey of the literature, Coles collected a considerable body of data on fluctuations in the sublayer. The results indicate that over a wide range of Reynolds number ($100 < \delta^+ < 10^4$), $u^{+\prime}_{max}$ has a nearly constant value of 2.75. At the same position $v^{+\prime}$ is about 0.6 and $w^{+\prime}$ is about 1.0. Using the "universal" numbers, $u^+/w^+ = 2.75$ as $y^+ \to 0$ and $\lambda^+ = 100$ plus Equation (3) matched to (4) and (2), Coles was able to produce a model of the secondary flow in the sublayer that gave excellent agreement with the collected measurements of $u^{+\prime}$, $v^{+\prime}$, $w^{+\prime}$, and $u'v'/\tau_w$ in the range $0 < y^+ < 15$.

(g) Discussion

Very few issues regarding the organized structure in the turbulent boundary layer could be considered resolved.[5] It is clear from the work of Corino & Brodkey, Kim et al, Willmarth, Grass, and others, that most of the production of turbulent energy near the wall occurs during

[5]The generally disordered state of our understanding of turbulent boundary-layer structure is well recognized by workers in the field. A useful step toward improving this situation with many good remarks identifying resolved as well as unresolved issues may be found in the summary of a recent Michigan State workshop on structure by Kline & Falco (1980).

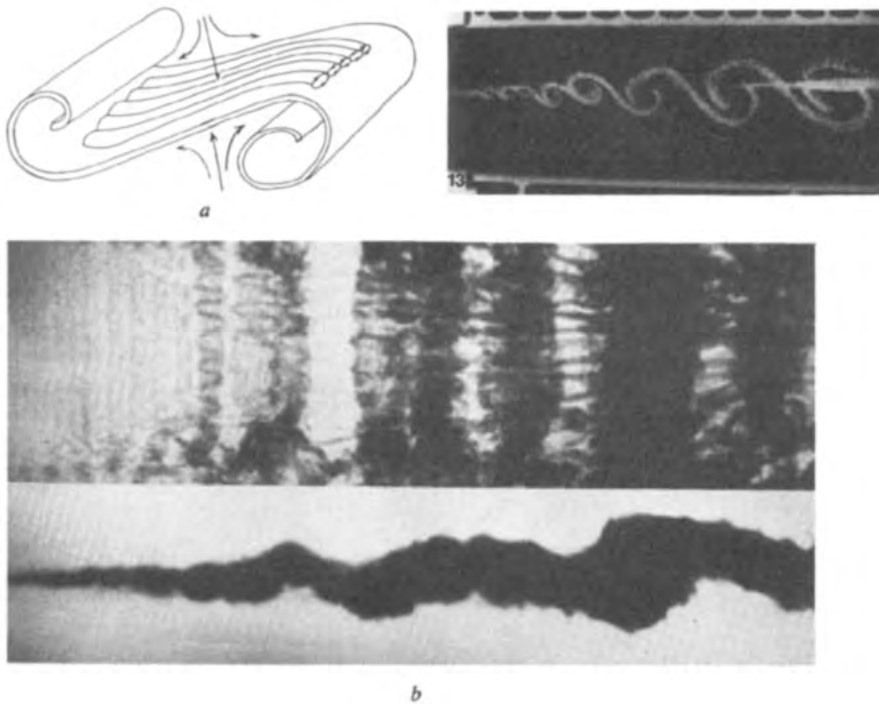

Figure 14 Three-dimensional structure in a plane mixing layer. (*a*) A conceptual picture from Corcos (1979). (*b*) A chemically reacting layer from Briedenthal (1978).

bursts. However, the interaction process that creates conditions under which bursts occur is very far from understood. It appears fairly well established that the mean time between bursts scales with outer variables. This is essentially a statement about the spacing between bursts in the streamwise direction as well as the rate at which bursts are produced at the wall, propagate, and decay. However, very little is known about the scaling laws for the spacing of bursts in the spanwise direction.

There is a variety of views regarding the interaction between inner and outer layers. In each case a causal relationship is drawn between different aspects of the organized structure. However, the elliptic nature of incompressible fluid motion makes cause and effect exceedingly difficult to distinguish and the hope is that, once a true understanding is reached, the need for such a distinction will vanish. Central to most views of the interaction process is the idea that bursts are the result of an inviscid instability of the instantaneous streamwise velocity profile (see Figures 5*a* and 6*b*). Inflection points in the instantaneous profile at

y^+ between 30 and 50 have been observed by Kline et al 1967, Smith 1978, and Blackwelder & Kaplan 1971. One view of the interaction (Rao et al 1971, Laufer & Narayanan 1971, and Kovasznay et al 1970) sees bursting as an instability of the sublayer produced by the pressure field associated with the large-scale motion in the outer layer. In another view (Offen & Kline 1974, 1975), the emphasis is on flow disturbances which move in from the logarithmic region much closer to the wall. In this view, sweeping motions from the log region impress on the wall the temporary adverse pressure gradient required to bring about the streak lifting that precedes a burst.

Another aspect of the interaction problem regards the maintenance of the outer flow. The predominant view is that the outer flow is in some sense the wake formed by a composite of successive bursts near the wall. Offen & Kline view the bulges in the outer flow as the result of vortex pairing between eddies associated with two to four bursts. In contrast, the observations of Rao et al and Narayanan & Marvin that the mean time between bursts is nearly independent of distance above the wall, suggests a single structure that fills the layer.

Scaling parameters for the length scales of streamwise vortices near the wall are well established to be ν and u^*. This is essentially guaranteed by the universality of the logarithmic shape of the velocity profile near the wall [Equation (4) for $y^+/\delta^+ \ll 1$]. However, the scaling of mean times between bursts on outer variables, plus the fact that bursts account for most turbulence production near the wall, contradicts this universality. Somehow the effect of, say, pressure gradient or roughness on bursting is manifested only through its effect on τ_w without any residual effect on the details of the shape of the velocity profile.

Scaling parameters for structural features of the outer portion of the boundary layers are much more in doubt. This arises from the fact that the effect of the wall is felt throughout the layer [recall Equation (10)]. As a result, any eddy structure in the outer layer will exhibit a dependence on wall variables. To see this consider the scaling properties of the Taylor and Kolmogorov microscales in the outer portion of the boundary layer. If production and dissipation of turbulent energy scale together in this region, then dimensional analysis leads to

$$\frac{\lambda}{\delta} \sim \frac{1}{R_\delta^{1/2}} \quad \text{and} \quad \frac{\eta}{\delta} \sim \frac{1}{R_\delta^{3/4}} \tag{19}$$

where λ and η are the Taylor and Kolmogorov microscales, respectively.[6]

[6]Unfortunately, λ is also used to denote sublayer streak scales which do not necessarily correspond to a Taylor microscale. To maintain the distinction, we use subscripted λ's ($\lambda_x, \lambda_y, \lambda_z$ to denote streak scales).

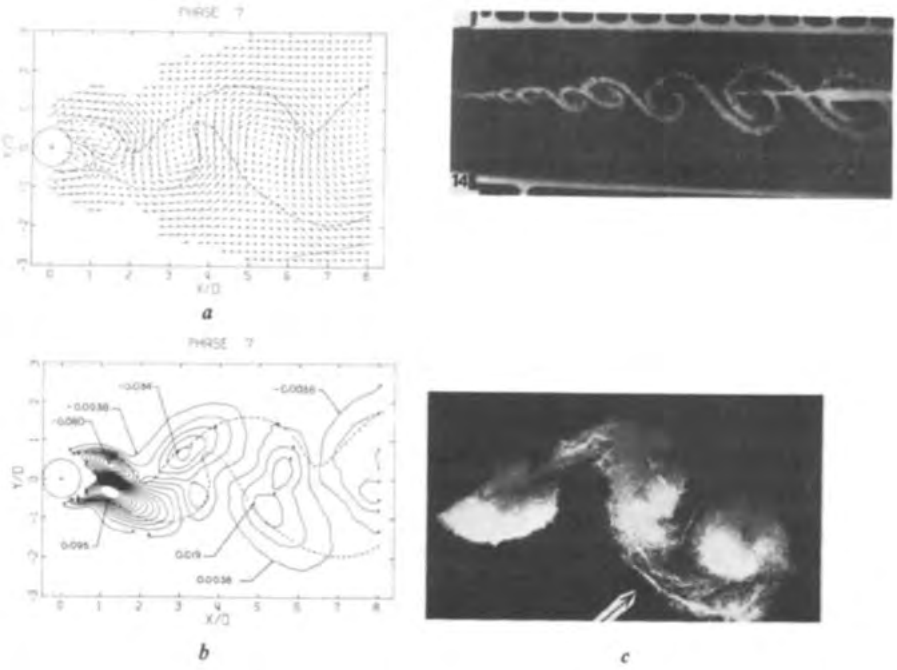

Figure 15 Ensemble-averaged mean flow at fixed phase in the cylinder near wake from B. J. Cantwell and D. E. Coles (1980 in preparation). (*a*) Mean flow referenced to an observer who moves downstream at 0.75 u_∞; (*b*) Shearing stress $\langle u'v' \rangle / u_\infty^2$ at constant phase; (*c*) Three-dimensional motions in the near wake of a flapped hydrofoil from Meijer (1965).

In a turbulent boundary layer we may write

$$\frac{\lambda u^*}{\nu} \sim \left(\frac{C_f}{2}\right)^{1/2} R_\delta^{1/2} \text{ and } \frac{\eta u^*}{\nu} \sim \left(\frac{C_f}{2}\right)^{1/2} R_\delta^{1/4}. \tag{20}$$

Making use of (10) we have

$$\frac{\delta u^*}{\nu} \sim e^{K\sqrt{\frac{2}{C_f}}}, \quad \frac{\lambda u^*}{\nu} \sim \left(\frac{C_f}{2}\right)^{1/4} e^{\frac{K}{2}\sqrt{\frac{2}{C_f}}},$$

$$\frac{\eta u^*}{\nu} \sim \left(\frac{C_f}{2}\right)^{3/8} e^{\frac{K}{4}\sqrt{\frac{2}{C_f}}}. \tag{21}$$

All three length scales depend exponentially on $1/C_f$, a quantity which increases very slowly with increasing x along the layer. Over typical ranges of C_f where observations are made both $\lambda u^*/\nu$ and $\eta u^*/\nu$

increase with decreasing C_f although the dependence on a fractional power of C_f mitigates the rate of increase somewhat. The dependence on C_f is somewhat stronger when δ, λ, and η are normalized on u_∞. Thus

$$\frac{\delta u_\infty}{\nu} \sim \left(\frac{2}{C_f}\right)^{1/2} e^{\kappa\sqrt{\frac{2}{C_f}}}, \quad \frac{\lambda u_\infty}{\nu} \sim \left(\frac{2}{C_f}\right)^{1/4} e^{\kappa\sqrt{\frac{2}{C_f}}},$$

$$\frac{\eta u_\infty}{\nu} \sim \left(\frac{2}{C_f}\right)^{1/8} e^{\kappa\sqrt{\frac{2}{C_f}}}. \tag{22}$$

Here the dependence on a power of $1/C_f$ leads to a faster rate of increase with decreasing C_f. Thus as far as eddy length scales are concerned, normalization with wall variables will invariably lead to a slower dimensionless rate of change with C_f or, equivalently, with Reynolds number. No experiment to date covers a broad enough range of Reynolds number to properly resolve the scaling laws for the flow structure in the outer layer. Moreover, the mean time between bursts $u_\infty T/\delta$ may also exhibit a weak dependence on wall variables when the range of Reynolds numbers has been extended. One of the most important needs for future research is to extend current observations to high Reynolds numbers, not so much to identify new transport mechanisms as Head & Bandyopadhyay (1978) suggest, but rather to establish the scaling laws for the mechanisms that are observed to play an important role at low Reynolds numbers.

III ORGANIZED MOTION IN FREE SHEAR FLOWS

In a study of transition in a laminar free shear layer, Freymuth (1966) noted the presence of highly regular vortex motions in the nonlinear stages of transition. He observed that the onset of subharmonic wavelengths was associated with an interaction he called "slip" in which two adjacent vortices rotate about a common axis and coalesce into a single structure. Downstream, the regular vortices appeared to give way to a chaotic motion. Traditionally, the breakdown to random, three-dimensional motion has been argued on the basis of vortex stretching along the principal axis of strain of the mean velocity field. Taking the curl of the momentum equation leads to the equation for vorticity

$$\frac{\partial \omega_i}{\partial t} + \frac{\partial}{\partial x_j}(u_j \omega_i) = \omega_i \frac{\partial u_i}{\partial x_j} + \nu \frac{\partial^2 \omega_i}{\partial x_j \partial x_j}. \tag{23}$$

The first term of the right-hand side of (23), the vortex stretching term,

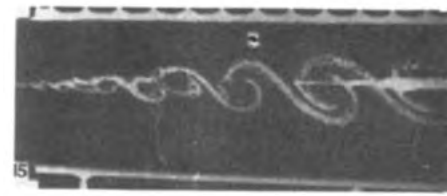

Figure 16 Oil slick from the tanker, Argo Merchant, grounded off the Nantucket Shoals in 1976 (Re$\sim 10^8$). Superimposed is the flow past an inclined flat plate at Re$= 10^3$.

acts as a source term for vorticity. Any spanwise vorticity, it could be argued, would be quickly dominated by much more intense vorticity in the streamwise direction. Furthermore, the streamwise vortex motions would contain most of the turbulent energy and any transverse vorticity would contribute little to the dynamics of the flow.

In a study of the turbulent mixing layer, Brown & Roshko (1974) discovered that the layer was dominated by large-scale spanwise vortex motions. These motions originate in the transitional part of the layer; they do not vanish when smaller-scale turbulence sets in and they appear to remain as a permanent feature of the flow at all higher Reynolds numbers. Winant & Browand (1974) carried out a detailed study of the vortex pairing observed by Freymuth in a low-Reynolds-number shear flow. In pairing, adjacent vortices rotate about each other under their mutual induced velocity field. As the rotation progresses they amalgamate into a single vortex of larger scale. Winant & Browand suggest that pairing is the principal mechanism by which a shear layer grows. A similar pairing process was observed by Brown & Roshko at much higher Reynolds number. A sequence of pictures from a movie taken by the Caltech group showing a pairing event is shown in the upper right-hand corner of the pages of this review (see also Roshko 1976). An x-t diagram of eddy trajectories showing the amalgamation of two and sometimes three vortices is shown in Figure 13*a*. Figure 13*b* shows eddy trajectories in the initial shear layer of an axisymmetric jet measured by Bouchard & Reynolds (1978). Here, vortex centers can be observed to orbit about each other several times before coalescing.

The picture of the mixing layer which emerges from this is of a double structure composed of an array of moving and interacting large-scale spiral vortex motions superimposed on a background of finer-scale, presumably random, turbulence. Although the persistence of these eddies remains a subject of some controversy (Chandrasuda et al 1978), there is ample evidence that they are present and play an important role at Reynolds numbers far above those at which the mixing layer would be considered transitional (Dimotakis & Brown 1976). In some ways, recent observations confirm several of the ideas of Townsend who had proposed a similar double structure with fine-scale turbulence convected about by eddies whose size was comparable to the overall scale of the flow. However, the large eddies were only vaguely perceived as a field of randomly interacting, slow moving, three-dimensional motions. The observations in the mixing layer gave symmetry and form to the conceptual picture of the large-scale structure of turbulent flow. Suddenly it was feasible and reasonable to draw a picture of turbulence! The hand, the eye, and the mind were brought into a new relationship that had never quite existed before; cartooning became an integral part of the study of turbulence.

Observations of the plane mixing layer stimulated a renewed interest in modeling unsteady viscous flow using discrete vortex arrays. This method had been used by Abernathy & Kronauer (1962) to model the laminar vortex street in a two-dimensional wake. Now it was resurrected as a method for modeling the large-scale motion in turbulence.[7] The essential idea here is to lump the continuous field of vorticity into individual vortex elements. The time evolution of the flow is then simulated by solving a set of first-order ordinary differential equations

$$\frac{dx_i}{dt} = \sum_{\substack{j=1 \\ i \neq j}}^{N} u_j(x_i, t) \tag{24}$$

where x_i is the coordinate of the ith vortex point and u_j is the velocity induced at x_i by the jth vortex point. Since the flow outside each vortex core satisfies Laplace's equation, the velocity induced at x_i is found by superposition. The method has been used in both two and three dimensions to model a number of flows including vortex sheet roll-up (Chorin & Bernard 1973), mixing layers (Ashurst 1977), wakes (Clements 1973,

[7] In remarkable anticipation of later observations, Onsager (1945) used the Hamiltonian structure of the equations of motion to analyze probable states for an array of point vortices. When the "temperature" of the array is negative, point vortices of the same sign tend to organize into large compound vortices. For more discussion, see the recent review by Saffman & Baker (1979).

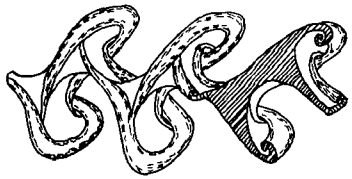

a

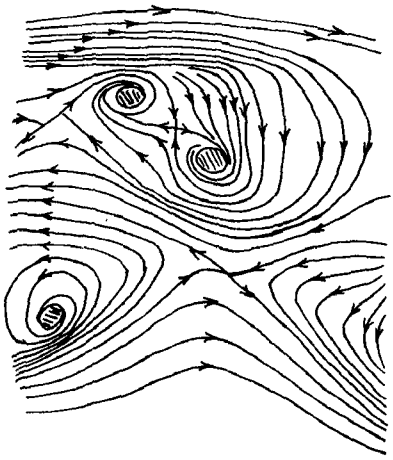

b

Figure 17 Flow patterns in three-dimensional flows from Perry, Lim & Chong (1980). (*a*) Smoke geometry of a neutrally buoyant wake structure. (*b*) Schematic representation of streamlines in a three-dimensional wake. (*c*) Smoke rising from a cigarette. (*d*) Smoke rising from a chimney.

c

d

Sarpkaya 1975), and turbulent spots (Leonard 1979). Generally, the simulations reproduce the large-scale motions in these flows remarkably well. However, they tend to do less well at simulating the associated stresses. At least part of the reason for this appears to be due to the neglect of small-scale three-dimensional motions, which contribute significantly to the stress.

Observations of organized structure in free-shear flows are not limited to mixing layers. Crow & Champagne (1971) observed quasi-deterministic motions in the developed portion of an axisymmetric jet. Bevilaqua & Lykoudis (1971) observed dye entrained into a two-dimensional wake and concluded that the interface convolutions visible on photographs of wakes are the outer edges of large vortices and that it is vortex induction by these large eddies that is primarily responsible for the entrainment of laminar fluid by the wake.

All of the evidence discussed so far is for organized motion at the largest scale of the flow superimposed on random background turbulence. However, there is an increasing amount of evidence for a high degree of order at smaller scales. Observations of highly organized three-dimensional motions in the mixing layer have been reported by Briedenthal (1978) who examined a chemically reacting flow in water. Figure 14*b* shows simultaneous side and top views of the flow. The large transverse eddies are strung together by a spaghetti-like net of small-scale streamwise counter-rotating vortices not unlike the streamwise vortices found near the wall under a turbulent boundary layer.

A flow that has been known to be dominated by coherent vortex motions for a long while is the near wake of a bluff body. Here the eddies are produced in a constant, regular manner and, except for some dispersion, are not subject to pairing or any other strong interaction that would obscure their identity. Measurements taken at a constant phase of the vortex-shedding cycle (B. J. Cantwell and D. E. Coles 1980, in preparation) are shown in Figure 15. Figure 15*a* shows the velocity field referenced to an observer who moves downstream with the vortices. In this frame of reference, the flow is quasi-steady and the organized motion is manifested as a pattern of centers and saddles. Similar patterns of the instantaneous velocity field in the wake of a bluff body have been measured by Davies (1976; D-shaped cylinder), Owen & Johnson (1978; circular cylinder at $M=0.6$), and Perry & Watmuff (1979; three-dimensional wake of an ellipsoid).

Some indirect evidence for organized small-scale structure can be found in the cylinder near wake depicted in Figure 15*b*. The stresses associated with the background turbulence in this flow are found to be comparable to the stresses due to the periodic large-scale motion (taken as a fluctuation away from the globally averaged mean flow). The background normal stresses $\langle u'^2 \rangle$ and $\langle v'^2 \rangle$ show expected behavior with maxima near vortex centers and minima between vortices. However, the background shearing stress $\langle u'v' \rangle$ shown in Figure 15*b* achieves a maximum in the saddle region between the vortices. If one forms the

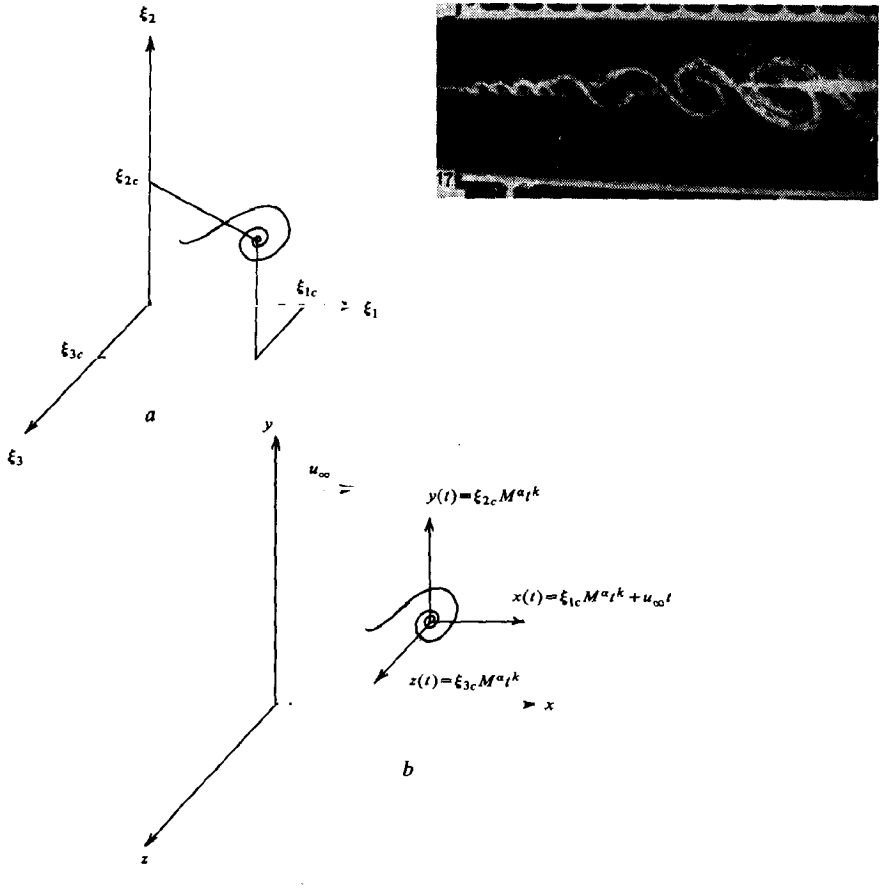

Figure 18 Trajectory of a nonsteady critical point in physical coordinates.

correlation coefficient

$$R=\frac{\langle u'v'\rangle}{(\langle u'^2\rangle)^{1/2}(\langle v'^2\rangle)^{1/2}} \tag{25}$$

it is found that near a vortex center, where the vorticity and turbulent energy are at their maximum, R is about 0.1, whereas, in the region of the saddle-point flow between vortices, where the background turbulent energy is at a minimum and where the transverse component of ensemble mean vorticity is nearly zero, R is between 0.5 and 0.6. The background turbulence in this flow is neither small nor random. It has structure. Vortex stretching due to the straining motion at the saddle must lead to a substantial strengthening of the component of vorticity

aligned with the diverging separatrix of the saddle. Some evidence for this effect is shown in the photograph of the wake of a supercavitating hydrofoil shown in Figure 15*c* where well-defined lines of cavitation bubbles connecting adjacent large eddies indicate a low-pressure zone associated with intense, highly stretched vorticity.

In a sense these observations also confirm some early views of turbulence in which the energy-containing eddies lie along the principal axis of strain of the mean velocity field. The main and very important difference is that the streamwise vortices convect with the flow responding, not to the stationary mean flow, but to the unsteady strain field imposed by the large eddies. Through the coupling between the large-scale motion and background turbulence the flow is differentiated into convecting regions of active and passive turbulence.

The question that immediately arises is, At what scale does organized motion in turbulent flow cease? Corcos (1979) has recently proposed a model for the plane mixing layer in which the flow is treated as essentially deterministic at all scales. The result is a cartoon of the mixing layer (Figure 14*a*), in which flattened streamwise vortices with thickness comparable to the Taylor microscale form in a perturbed saddle-point flow between adjacent large-scale vortices. The prospect raised here is that the physics of turbulent flow can be understood and modeled by considering an equivalent small number of complex laminar flows. If this is so, then many traditional ideas about turbulence, for example the concept of local isotropy and the cascade picture of turbulent energy exchange between large and small scales, need to be re-examined in light of the possibility that even very small-scale motions may be highly organized. Old ideas will not be discarded, but they will receive a new, more illuminating, physical interpretation.

An area of active current research, which has been stimulated by observations of organized motion in both wall-bounded flows and free-shear flows, is large-eddy simulation. The basic approach here (Reynolds 1976) is to compute large-scale unsteady motions explicitly while modeling only those motions that lie at scales below that which can be resolved by the computational grid. Several flows have been simulated thus far with encouraging results. Calculations of homogeneous and isotropic turbulence were used by Clark et al (1979) to generate "empirical" constants for Reynolds-stress models which previously could only have been determined from measurements of grid turbulence. Large-eddy simulation of turbulent channel flow by Moin et al (1978) reproduced mean velocity profiles (particularly the logarithmic portion near the wall) which were in good agreement with the measurements of Hussain & Reynolds (1975). In addition, the calculations

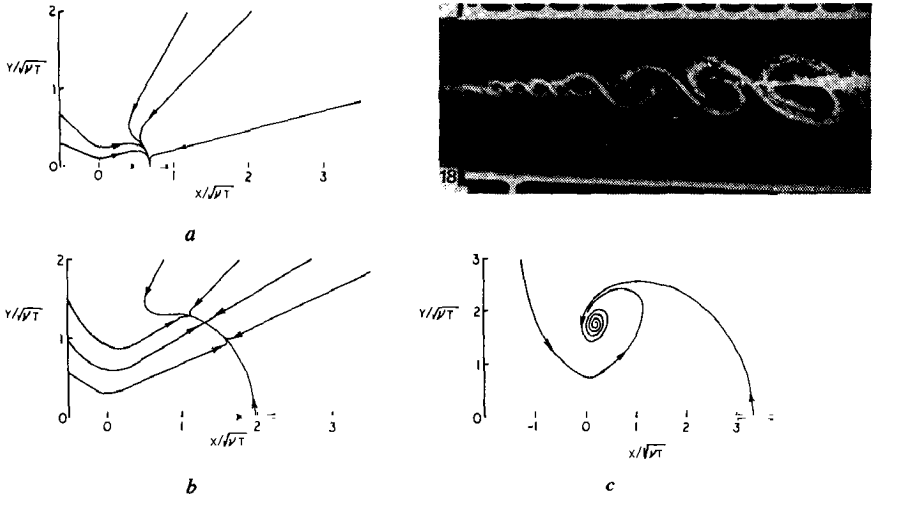

Figure 19 Entrainment diagrams for the solution of the creeping round jet at (*a*) Re=2.0, (*b*) Re=8.0, (*c*) Re=20.0.

yielded data for quantities such as pressure and pressure-velocity correlations that cannot be measured experimentally.

At the heart of this approach is the assumption that unresolved sub-grid-scale fluctuations are only slightly nonisotropic and can be modeled in a universal way. The cutoff between large and small scales is essentially a function of the current state of computer technology. As machines become larger and faster (as they have and will become) the fraction of the spectrum of energy containing turbulent motions that can be computed explicitly will grow toward one. However, even the most optimistic forecaster of this evolution would concede that the technology-imposed cutoff between large and small scales will never approach the order of the Kolmogorov scale in a high-Reynolds-number, aerodynamically useful flow. A grid of this resolution in a given volume would require $N \cong \mathrm{Re}^{9/4}$ where N is the number of grid points and Re is the Reynolds number of the flow in question based on global velocity and length scales. For a 4-cm chord compressor blade at 400 m/sec ($\mathrm{Re} \simeq 10^6$) N equals 3×10^{13}. For a 200-cm airfoil at the same speed ($\mathrm{Re} \simeq 5 \times 10^7$) N equals 2×10^{17}. However, estimates of the largest memory sizes available by the end of the century (Chapman 1979) do not exceed $N = 10^{11}$ (a four-order-of-magnitude increase in size over today's largest memories). The above estimate of N is rather pessimistic. One may only need to resolve a Taylor microscale, in which case $N \sim \mathrm{Re}^{3/2}$. In addition, efficient grid-generating schemes can be used to reduce N substantially.

In any case, for the foreseeable future, large-eddy simulation of high-Reynolds-number turbulent flows will have to stop at scales that will be several orders of magnitude greater than the smallest scales in the flow. In this respect the observations of small-scale organized motion raise a number of critical questions. Are these motions small in the sense of a Taylor or Kolmogorov microscale or are they really of intermediate scale? How is the coupling between large and small scales really accomplished? Is the motion at small scales the same from flow to flow? What is the maximum scale size at which local isotropy begins to be valid and will computers ever be able to see this scale for flows of engineering importance?

IV TRANSITION AND THE CONTROL OF MIXING

More and more evidence has accumulated in the past few years that shows that virtually all turbulent shear flows are sensitive to transition, or more precisely, to perturbations applied during transition. Traditionally, it was believed that sufficiently far from their point of origin turbulent shear flows would reach an asymptotic state in which their rate of growth and decay would become independent of the manner in which the flow was started (see, for example, Liepmann 1962). The overwhelming body of data shows that once turbulence is established the overall properties of turbulent shear flows away from solid boundaries are virtually independent of viscosity. Although viscosity is essential to the creation of turbulence it seems to serve only to establish smaller and smaller scales of motion with more and more intense velocity gradients sufficient to dissipate the increased rate of energy input as the Reynolds number is increased. However, the Taylor microscale is usually associated, on dimensional grounds, with a velocity perturbation comparable to that associated with the largest eddies. It is not at all obvious that the overall behavior of the flow can depend so little on Reynolds number in the presence of such intense motions that depend strongly on Reynolds number.

The same data that demonstrates the Reynolds-number invariance of turbulence (illustrated by Figure 16) also shows very wide scatter (Roshko 1976). The mixing-layer spreading rates measured by Winant & Browand for $u_2/u_1=0.4$ at a streamwise Reynolds number of 10^4 are in close agreement with the measurements of Spencer & Jones (1971) at a Reynolds number of 10^6. In contrast, the spreading rate measured by Wygnanski & Fiedler (1970) at $\mathrm{Re}=5\times10^5$ differs by 30% from the value measured by Liepmann & Laufer (1947) for $u_2/u_1=0$ at a

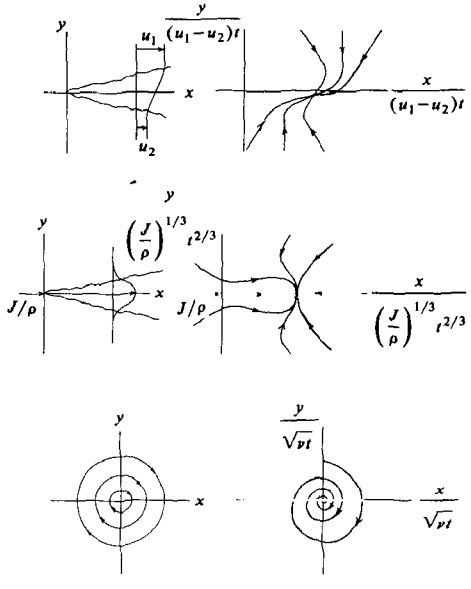

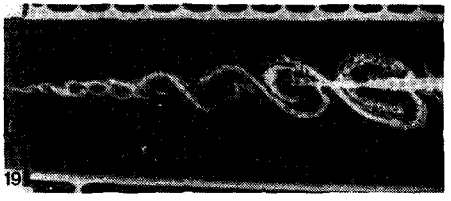

Figure 20 Entrainment diagrams for several flows. (*a*) The stationary turbulent mixing layer; (*b*) The stationary plane turbulent jet; (*c*) The Oseen viscous vortex.

Reynolds number of 10^6. Batt (1975) suggests that this is related to the presence or absence of a boundary-layer trip on the splitter plate ahead of the origin of the layer. As Roshko points out, much of the evidence suggests that any important effects of Reynolds number appear indirectly through conditions affecting transition rather than through the direct action of viscosity on the developing turbulent structure. In a recent evaluation of shear-layer data, Birch (1980) has suggested that much of the scatter in measurements of shear-layer spreading rate can be attributed to variations in the effective origin of the layer.

Effects of initial conditions have been observed by Leonard (1979) in numerical simulations of developing turbulent spots. In this study the spot is imbedded in an initially planar array of transverse vortex lines (Figure 9*b* and *c*). He finds that the downstream amplitude distribution of the distorted and stretched vortex lines appears to be directly related to the amplitude distribution of the initial disturbance.

Furuya & Osaka (1976) examined the effect of a distribution of roughness placed near the leading edge of a flat-plate zero-pressure-gradient turbulent boundary layer. Measurements of the spanwise distribution of momentum thickness showed a variation that was directly related to the spanwise variation of roughness. When the measurements were made several thousand boundary-layer thicknesses downstream, the same spanwise distribution of momentum thickness was found. Instead of decaying with distance, the amplitude of the variation had

increased. In fact, the variation simply scaled with the boundary-layer thickness. Apparently the effect of roughness placed near the plate leading edge is to produce a permanent change in the large structure of the layer.

Other evidence that shear flows are sensitive to small perturbations may be found in the probe interference effects on shear layers observed by Hussain & Zaman (1978). They found that when a hot-wire probe was inserted into a laminar free-shear layer, it was found to induce stable edge-tone-like upstream oscillations. Their results suggest that a reference probe used near the origin of a free shear layer can alter the basic instability frequency of the layer, in turn influencing the downstream development of the coherent structure.

The sensitivity of shear flows to small perturbations applied during transition, together with the recognition that the developed flow is dominated by organized structures which appear to be remnants of transition, are the ingredients that suggest that some form of control over turbulent mixing may be possible. Oster et al (1977) were able to exert remarkable open-loop control on a plane mixing layer by flapping a small spanwise ribbon just downstream of the end of the splitter plate in the initial region of the layer. By adjusting the amplitude and frequency of the oscillation, they were able to halve or double the angle of spread of the layer. Under certain conditions the layer would spread for a while, stop spreading for a short distance, and then begin spreading again. The vibrating ribbon strongly influences the rate and phase at which vorticity is injected into the flow. The result is controlled vortex formation reminiscent of the "locking on" of vortex shedding observed to occur on vibrating bluff bodies (Griffin & Ramberg 1974). One can easily envision the use of effects of this kind in a closed-loop system where the flow is sensed and a perturbation is applied to produce some desired change in the flow. There is little doubt that the next few years will see a great deal of fruitful research in this area.

Are turbulent eddies like tennis balls or like medicine balls? It was once felt that an initially perturbed flow would rebound and eventually reach a unique asymptotic state. It now appears that an initially perturbed turbulent flow may remain permanently perturbed; that it may have an infinity of possible asymptotic states corresponding to an infinite variety of perturbed initial states. If this is so, then tremendous benefits may be realized through the control of mixing. However, it complicates our theoretical understanding. It is no longer enough to predict the angle of spread of a mixing layer; now we must be able to predict all possible angles of spread as a function of initial conditions.

This issue is still far from resolved and points up the need for standards for taking data. Present and future measurements need to be carefully and accurately scaled. In particular, it is necessary to distinguish between differences in flow conditions, methods of data presentation and reduction, and true differences in state.

V ENTRAINMENT DIAGRAMS

A glossary of terms used to describe the coherent structure in turbulent flows would be long indeed. There are bursts, sweeps, streaks, typical eddies, streamwise vortices, transverse vortices, large eddies, etc. Every term is used to describe some structural feature of the motion. One of the central problems in current research is to relate these usually observed features to the usually not observed variables of fluid motion; streamlines, streaklines, pathlines, pressure, and their various derivatives.

The unsteady patterns of centers and saddles observed in conditionally averaged turbulent flow have much in common with the phase portraits of nonlinear dynamical systems. The connection is through the equations for particle paths,

$$\frac{dx_i(t)}{dt} = u_i(\mathbf{x}(t), t). \tag{26}$$

If a frame of reference can be found in which the flow is steady, then (26) reduces to an autonomous system with integral curves that coincide with the streamlines of the velocity field referred to the same frame. A number of authors have made use of this fact to explore the properties of solution trajectories in a variety of steady-flow situations. Oswatitsch (1958) and Lighthill (1963) classified certain critical points which can occur near a rigid boundary. Perry & Fairlie (1974) reviewed critical-point analysis in a general way and applied the technique to the problem of three-dimensional separation. They placed special emphasis on the fact that the method provides a wealth of topological language particularly well suited to the description of fluid-flow patterns. Recently Hunt et al (1978) applied critical-point theory to flow-visualization studies of bluff obstacles. More recently, Peake & Tobak (1980) reviewed the use of critical-point theory as it is applied to the study of three-dimensional vortex flows about various bodies in high-speed flow.

The success of critical-point theory for studying steady flow, coupled with the observations of organized spiral vortex motions in unsteady flows (critical-point-like motions) have led to a search for ways to

extend the theory to unsteady flow. Perry & Lim (1978) used critical-point analysis to produce a qualitative description of the three-dimensional unsteady flow patterns in co-flowing jets and wakes (Figure 17*a* and *b*). Pullin (1978) studied the evolution of critical points in the unsteady streamline pattern associated with vortex-sheet rollup from the edge of an impulsively started plate.

The instantaneous streamline patterns used for these analyses provide a form of flow visualization combined with substantial amounts of quantitative information about the flow. Most importantly, they focus on the problem of connecting vortex structures together to complete the flow field. However, there are significant conceptual problems involved in interpreting unsteady streamline patterns as they relate to entrainment. In an unsteady flow, streamlines can move across fluid pathlines; thus the stream function provides little insight into the behavior of the fluid itself. Furthermore, structural features of the flow often remain hidden in a picture of instantaneous streamlines.

Particle trajectories plotted in physical coordinates also present similar conceptual difficulties. If the integration of the particle-path equations is carried out over a volume of particles, then each point in space will be traversed by an infinite set of trajectories, each with a different slope corresponding to the passage of particles through the point at successive instants of time. In addition, the pattern of particle paths, like the pattern of streamlines, depends on the frame of reference. For a recent appreciation of this problem see Lugt (1979).

Certain time-dependent flows can be reduced to a self-similar form. Such flows usually depend on one or at most two global parameters. In this case, some of the above objections can be removed by reducing the particle-path equations (26) to an autonomous system in similarity coordinates. Figure 11*c* is a diagram of particle trajectories in similarity coordinates used to analyze the flow structure on the plane of symmetry of a turbulent spot. Particle trajectories in similarity coordinates were used by Turner (1964) to analyze the flow pattern in a rising turbulent thermal which was modeled using an expanding Hill's spherical vortex. This method can be used to generate entrainment diagrams for a wide variety of shear flows, some steady, some unsteady, some laminar, and some turbulent. Some of the flows are governed by the Navier-Stokes equations, some by the boundary-layer equations, and some by the Oseen equation. In most cases the transformations involve simple stretchings, although more complex transformations involving uniform and logarithmic rotations and arbitrary nonuniform translations (Cantwell 1978) are allowed. In fact, it appears that virtually every incompressible viscous flow that we ordinarily think of as self-similar in

space (the Blasius boundary layer, the round jet, the plane turbulent mixing layer, etc) can be thought of as a special case of a more general unsteady flow that is self-similar in time with particle paths which reduce to an autonomous system. In the general case the flow is assumed to have been started at some initial time. Table 2 summarizes various similarity transformations and the reduced equations that may be derived from them. The basic similarity variable is

$$\xi_i = \frac{x_i - V_i t}{M^\alpha t^k} \tag{27}$$

where M is an invariant of the motion with units $L^m T^{-n}$ and α and k are chosen so that $M^\alpha t^k$ has the dimensions of a length. Thus

$$\alpha = 1/m, \; k = n/m. \tag{28}$$

Included are flows where there is a uniform velocity to the right in the x-direction so that $V=(u_\infty,0,0)$ and flows where there is no externally imposed velocity $V=(0,0,0)$. Consider the trajectory of a critical point shown schematically as a stable focus in Figure 18. If we take ξ_1 in the direction of the external flow, and ξ_2 and ξ_3 as cross-stream directions, then in physical coordinates, the trajectory of the critical point is given by

$$x_c = u_\infty t + \xi_{1c} M^\alpha t^k, \; y_c = \xi_{2c} M^\alpha t^k, \; z_c = \xi_{3c} M^\alpha t^k, \tag{29}$$

for flows governed by the full equations, by

$$x_c = \xi_{1c} M^\alpha t^k, \; y_c = \xi_{2c} \sqrt{\nu t}\,, \; z_c = \xi_{3c} \sqrt{\nu t}\,, \tag{30}$$

for flows governed by the boundary-layer equations, and by

$$x_c = u_\infty t + \xi_{1c} M^\alpha t^k, \; y_c = \xi_{2c} \sqrt{\nu t}\,, \; z_c = \xi_{3c} \sqrt{\nu t}\,, \tag{31}$$

for flows governed by the Oseen equation.

If we take $\delta = \sqrt{y_c^2 + z_c^2}$ as a cross-stream length scale and $u_0 = u_\infty - \dot{x}_c$ as a characteristic streamwise velocity scale, then the four cases listed in Table 1, item 5, may be distinguished. Using the relations in Table 1, plus the parameters that are used to characterize various shear flows, one can construct Table 2. The important point in all of the above is the connection between turbulence structure and specific structural details of the velocity field. The concept of organized structure is advanced to a description in terms of critical points in the entrainment diagram and their relationship to the propagation and decay of the flow.

For turbulent flows the time evolution of scales is given by

$$\delta \sim M^\alpha t^k, \; u_0 \sim k M^\alpha t^{k-1}. \tag{32}$$

Essential to the self-similar development of turbulent flows is the

Table 1 Equations and self-similar forms

Full equations of motion	Boundary-layer equations	Oseen equations
	$\frac{\partial p}{\partial y}=0$	$\frac{\partial p}{\partial y}=0$
$\frac{\partial u_i}{\partial x_i}=0$	$\frac{\partial u}{\partial x}+\frac{\partial v}{\partial y}=0$	$\frac{\partial u}{\partial x}+\frac{\partial v}{\partial y}=0$
$\frac{\partial u_i}{\partial t}+u_j\frac{\partial u_i}{\partial x_j}=-\frac{1}{\rho}\frac{\partial p}{\partial x_i}+\frac{1}{\rho}\frac{\partial \tau_{ij}}{\partial x_j}$	$\frac{\partial u}{\partial t}+u\frac{\partial u}{\partial x}+v\frac{\partial u}{\partial y}=-\frac{1}{\rho}\frac{\partial p}{\partial x}+\nu\frac{\partial^2 u}{\partial y^2}$	$\frac{\partial u}{\partial t}+u_\infty\frac{\partial u}{\partial x}=\nu\frac{\partial^2 u}{\partial y^2}-\frac{1}{\rho}\frac{\partial p}{\partial x}$
(1) Similarity variables		
$\xi_i=\frac{x_i-V_i t}{M^{\alpha_t}t^k}$	$\xi=\frac{x}{M^{\alpha_t}t^k}$	$\xi=\frac{x-u_\infty t}{M^{\alpha_t}t^k}$
$U_i(\underline{\xi})=\frac{u_i-V_i}{M^{\alpha_t}t^{k-1}}$	$\eta=\frac{y}{\sqrt{\nu t}}$	$\eta=\frac{y}{\sqrt{\nu t}}$
$P(\underline{\xi})=\frac{p}{\rho M^{2\alpha_t}t^{2k-2}}$	$U(\xi,\eta)=\frac{u}{M^{\alpha_t}t^{k-1}}$	$U(\xi,\eta)=\frac{u-u_\infty}{M^{\alpha_t}t^{k-1}}$
$T_{ij}(\underline{\xi})=\frac{\tau_{ij}}{\rho M^{2\alpha_t}t^{2k-2}}$	$V(\xi,\eta)=\frac{vt^{1/2}}{\nu^{1/2}}$	$V=\frac{vt^{1/2}}{\nu^{1/2}}$
	$P(\xi,\eta)=\frac{p}{\rho M^{2\alpha_t}t^{2k-2}}$	$P(\xi,\eta)=\frac{p}{\rho M^{2\alpha_t}t^{2k-2}}$
(2) Reduced equations		
	$\frac{\partial P}{\partial \eta}=0$	$\frac{\partial P}{\partial \eta}=0$
$\frac{\partial U_i}{\partial \xi_i}=0$	$\frac{\partial U}{\partial \xi}+\frac{\partial V}{\partial \eta}=0$	$\frac{\partial U}{\partial \xi}+\frac{\partial V}{\partial \eta}=0$
$(k-1)U_i+(U_j-k\xi_j)\frac{\partial U_j}{\partial \xi_j}=-\frac{\partial P}{\partial \xi_i}+\frac{\partial T_{ij}}{\partial \xi_j}$	$(k-1)U+(U-k\xi)\frac{\partial U}{\partial \xi}+\left(V-\frac{\eta}{2}\right)\frac{\partial U}{\partial \eta}=-\frac{\partial P}{\partial \xi}+\frac{\partial^2 U}{\partial \eta^2}$	$(k-1)U-k\xi\frac{\partial U}{\partial \xi}-\frac{\eta}{2}\frac{\partial U}{\partial \eta}=\frac{\partial^2 U}{\partial \eta^2}-\frac{\partial P}{\partial \xi}$

(3) Pathline equations

$$\frac{d\xi_i}{d\tau} = U_i(\underline{\xi}) - k\xi_i \qquad \tau = \ln t$$

$$\frac{d\xi}{d\tau} = U(\xi,\eta) - k\xi \qquad \frac{d\eta}{d\tau} = V(\xi,\eta) - \frac{\eta}{2} \qquad \tau = \ln t$$

$$\frac{d\xi}{d\tau} = U(\xi,\eta) - k\xi \qquad \frac{d\eta}{d\tau} = V(\xi,\eta) - \frac{\eta}{2} \qquad \tau = \ln t$$

(4) Temporal scaling laws

for δ and u_0

$$\delta \sim t^k \qquad u_0 \sim t^{k-1}$$

$$\delta \sim t^{1/2} \qquad u_0 \sim t^{k-1}$$

$$\delta \sim t^{1/2} \qquad u_0 \sim t^{k-1}$$

(5) Spatial scaling laws

for δ and u_0

Case 1. Jet-like $V=(0,0,0)$

$$\delta \sim x \qquad u_0 \sim x^{1-1/k}$$

Case 2. Wake-like $V=(u_\infty,0,0)$

$$\delta \sim x^k \qquad u_0 \sim x^{k-1}$$

Case 3. Jet-like boundary layers

$$\delta \sim x^{1/2k} \qquad u_0 \sim x^{1-1/k}$$

Case 4. Wake-like boundary layers

$$\delta \sim x^{1/2} \qquad u_0 \sim x^{k-1}$$

Note: M is a parameter of the motion with units $L^m T^{-n}$ and $\alpha = 1/m$, $k = n/m$.

Note: δ is a characteristic cross-stream length scale.
u_0 is a characteristic stream-wise velocity scale.

Table 2 Growth and decay laws for shear flows

Class/Flow	Invariant	Parameter	Units	Exponent in time	Exponent in space	
				k	δ	u_0
Jet-like						
Plane mixing layer	u_0—velocity difference	u_1-u_2	LT^{-1}	1	1	0
Turbulent spot	u_0—free stream velocity (neglect variation in C_f)	u_∞	LT^{-1}	1	1	0
Turbulent boundary layer	u_0—free stream velocity (neglect variation in C_f)	u_∞	LT^{-1}	1	1	0
Plane plume	u_0^3—2-D buoyancy flux	B	L^3T^{-3}	1	1	0
Round plume	$u_0^3\delta$—3-D buoyancy flux	B	L^4T^{-3}	3/4	1	−1/3
Vortex sheet rollup	$u_0\delta^{1/2}$—potential flow parameter	γ	$L^{3/2}T^{-1}$	2/3	1	−1/2
Plane jet	$u_0^2\delta$—2-D momentum flux	J	L^3T^{-2}	2/3	1	−1/2
Round jet	$u_0^2\delta^2$—3-D momentum flux	J	L^4T^{-2}	1/2	1	−1
Laminar round jet	$u_0^2\delta^2$, ν—3-D momentum flux, viscosity	ν	L^2T^{-1}	1/2	1	−1
Radial jet	$u_0^2\delta^2$—3-D momentum flux	J	L^4T^{-2}	1/2	1	−1
Laminar radial jet	$u_0^2\delta^2$, ν—3-D momentum flux, viscosity	ν	L^2T^{-1}	1/2	1	−1
Line vortex	$u_0\delta$—circulation	Γ	L^2T^{-1}	1/2	1	−1
Laminar line vortex	$u_0\delta$, ν—circulation, viscosity	ν	L^2T^{-1}	1/2	1	−1
Vortex pair	$u_0\delta^2$—2-D impulse	I	L^3T^{-1}	1/3	1	−2
Vortex ring	$u_0\delta^3$—3-D impulse	I	L^4T^{-1}	1/4	1	−3
Wake-like						
Plane wake	$u_0\delta$—2-D far wake drag	D	L^2T^{-1}	1/2	1/2	−1/2
Round wake	$u_0\delta^2$—3-D far wake drag	D	L^3T^{-1}	1/3	1/3	−2/3
Plane momentumless wake	$u_0\delta^3$—requires a model	—	L^4T^{-1}	1/4	1/4	−3/4
Round momentumless wake	$u_0\delta^4$—requires a model	—	L^5T^{-1}	1/5	1/5	−4/5
Grid turbulence initial decay	$u_0^2\delta^3$—Saffman invariant	S	L^5T^{-2}	2/5	2/5	−3/5

Jet-like boundary layer						
Laminar plane mixing layer	u_0, ν—velocity difference, viscosity	u_1-u_2	LT^{-1}	1	1/2	0
Laminar plane plume	u_0^3, ν—2-D buoyancy flux, viscosity	B	L^3T^{-3}	1	1/2	0
Laminar round plume	$u_0^3\delta$, ν—3-D buoyancy flux, viscosity	$B/\sqrt{\nu}$	$L^3T^{-5/2}$	5/6	3/5	−1/6
Laminar plane jet	$u_0^2\delta$, ν—2-D momentum flux, viscosity	$J/\sqrt{\nu}$	$L^2T^{-3/2}$	3/4	2/3	−1/3
Falkner Skan boundary layers	$u_0x^{-\beta}$, ν—-free stream parameter, viscosity	M	$L^{1-\beta}T^{-1}$	$1/(1-\beta)$	$(1-\beta)/2$	β
$\beta=0$ Blasius layer	u_0, ν—free stream velocity, viscosity	u_∞	LT^{-1}	1	1/2	0
$\beta=-1$ Jeffrey-Hamel flow	$u_0\delta$, ν—area flux, viscosity	Q	L^2T^{-1}	1/2	1	−1
Wake-like boundary layer						
Laminar round wake	$u_0\delta^2$, ν—3-D far wake drag, —viscosity	D/ν	L	0	1/2	−1

observation discussed earlier, drawn from the study of homogeneous and isotropic turbulence and confirmed empirically for shear flows, that the energy-containing flow structure does not depend directly on the value of the fluid viscosity; one can assume Reynolds number invariance. This assumption is intimately connected to the dependence of the flow Reynolds number on time

$$\mathrm{Re}_\delta = \frac{u_0\delta}{\nu} = \frac{kM^{2\alpha}}{\nu} t^{2k-1}. \tag{33}$$

For flows with $k=1/2$, inertial and viscous times scale together and the assumption is unnecessary. For flows with $k>1/2$ the inertial time will dominate at all but the smallest scales. However, flows with $k<1/2$ will tend to follow a viscous scale as time increases.

Now let us examine the behavior of small-scale motions. If we assume that production and dissipation scale together then dimensional analysis leads to

$$\frac{\lambda}{\delta} \sim \mathrm{Re}_\delta^{-1/2} \text{ and } \frac{\eta}{\delta} \sim \mathrm{Re}_\delta^{-3/4} \tag{34}$$

upon substitution of (32)

$$\lambda \sim \left(\frac{\nu t}{k}\right)^{1/2} \text{ and } \eta \sim \nu^{3/4} M^{-\alpha/2} k^{-3/4} t^{3/4-k/2}. \tag{35}$$

The main result here is that the time evolution of the Taylor microscale is always independent of the global parameter M.

The entrainment diagram is always invariant for moving observers. Under the assumption of nonsteady similarity, the global parameter M determines the appropriate value of k. Once k has been determined, the rate of convection and growth of structural features in the flow (critical points, turbulent interfaces, etc) is determined. If we choose to move (nonuniformly) with a coordinate system that remains attached to some preferred feature, then, in the moving coordinate system,

$$x_i' = x_i + a_i M^\alpha t^k,\ t' = t,\ u_i' = u_i + a_i k M^\alpha t^{k-1}, \tag{36}$$

and the similarity variables in moving coordinates are

$$\xi_i' = \xi_i + a_i,\ U_i(\xi') = U_i(\xi) + k a_i, \tag{37}$$

where a_i is a dimensionless rate of motion in the x_i direction.

It is clear from the above that the pattern formed by the velocity vector field will depend on the a_i. This is true whether one plots the u_i field in physical coordinates or the U_i field in similarity coordinates.

Similarly, the pattern of particle displacements, dx_i, in physical coordinates will depend on the a_i. However, the pattern of particle displacements in similarity coordinates, $d\xi_i$, is independent of the a_i. This follows from the form of the pathline equations in Table 1, item 3.

$$U_i(\xi)-k\xi_i=U_i'(\xi')-ka_i-k\xi_i'+ka_i=U_i'(\xi')-k\xi_i'. \tag{38}$$

Equation (38) is an important result for it states that the location and character of a critical point in similarity coordinates is fixed by the dynamics governing the flow and by the choice of a value for k (which is a consequence of the units of M) and not by the incidental choice of speed for a moving observer.

The above results form the framework for a powerful method for analyzing the *dynamics* of fluid motion. To illustrate this, let us examine the Reynolds-number dependence of an impulsively started, axisymmetric, laminar jet produced by a point momentum source of strength J/ρ. The Reynolds number of the jet is $\mathrm{Re}=(J/\rho)^{1/2}/\nu$. Dimensional considerations lead to a formulation of the problem in terms of similarity variables

$$\psi=\nu^{3/2}t^{1/2}g(\xi,\theta;\mathrm{Re}),\ \xi=r/\sqrt{\nu t} \tag{39}$$

where ψ is the Stokes stream function and r and θ are the radial distance and azimuthal angle in spherical polar coordinates. A solution for the creeping-flow limit $\mathrm{Re}\to 0$ due to Sozou (1979) is

$$g(\xi,\theta)=\frac{\mathrm{Re}^2}{16\pi}\sin^2\theta\left\{2\xi-\frac{4}{\sqrt{\pi}}e^{-\xi^2/4}-\left(2\xi-\frac{4}{\xi}\right)\mathrm{erf}\left(\frac{\xi}{2}\right)\right\}. \tag{40}$$

By all conventional measures (40) would appear to exhibit only a trivial dependence on Reynolds number. However, an examination of the entrainment diagram of (40) reveals a remarkably complex structure (Cantwell 1980). The equations for particle paths are

$$\frac{dr}{dt}=u(r,\theta,t;\mathrm{Re});\ \frac{d\theta}{dt}=\frac{v(r,\theta,t;\mathrm{Re})}{r} \tag{41}$$

or, in terms of similarity variables,

$$\frac{d\xi}{d\tau}=U(\xi,\theta;\mathrm{Re})-\frac{\xi}{2};\ \frac{d\theta}{d\tau}=\frac{V(\xi,\theta;\mathrm{Re})}{\xi} \tag{42}$$

where $\tau=\ln t$ and

$$U=\frac{1}{\xi^2\sin\theta}\frac{\partial g}{\partial\theta};\ V=-\frac{1}{\xi\sin\theta}\frac{\partial g}{\partial\xi}. \tag{43}$$

Substitution of (40) into (42) leads to

$$\frac{d\xi}{d\tau} = \frac{\mathrm{Re}^2}{2\pi}\frac{\cos\theta}{\xi^2}\left\{\frac{\xi}{2} - \frac{1}{\sqrt{\pi}}e^{-\xi^2/4} - \left(\frac{\xi}{2} - \frac{1}{\xi}\right)\mathrm{erf}\left(\frac{\xi}{2}\right)\right\} - \frac{\xi}{2}, \tag{44}$$

$$\frac{d\theta}{d\tau} = -\frac{\mathrm{Re}^2}{4\pi}\frac{\sin\theta}{\xi}\left\{\frac{1}{2} + \frac{1}{\xi\sqrt{\pi}}e^{-\xi^2/4} - \left(\frac{1}{2} + \frac{1}{\xi^2}\right)\mathrm{erf}\left(\frac{\xi}{2}\right)\right\}. \tag{45}$$

The structure of the flow is examined by finding and classifying critical points of (44) and (45); points (ξ_c, θ_c) at which both right-hand sides are equal to zero. The zeros of (45) are at ($\theta = 0, \pi$, all ξ) and ($\xi = 1.7633$, all θ) and are clearly the same for all Reynolds numbers. Setting the right-hand side of (44) equal to zero gives

$$\mathrm{Re}^2 = \frac{\pi\xi_c^3}{\left(\frac{\xi_c}{2} - \frac{1}{\sqrt{\pi}}e^{-\xi_c^2/4} - \left(\frac{\xi_c}{2} - \frac{1}{\xi_c}\right)\mathrm{erf}\left(\frac{\xi_c}{2}\right)\right)\cos\theta_c}. \tag{46}$$

Equation (46) defines a family of curves in the (ξ, θ) plane for various values of the Reynolds number. Intersections between (46) and the zeros of (45) locate critical points in the entrainment diagram of the solution (40). From the above discussion, it is clear that, in spite of the apparently trivial Reynolds-number dependence of the streamline pattern of (40), the entrainment diagram may exhibit a Reynolds-number dependence that is quite complex. Figure 19 shows the entrainment diagram of (40) at three values of the Reynolds number. For sufficiently small Reynolds number, pathlines converge to a single stable node which lies on the axis of the jet. At a Reynolds number of 6.7806 the pattern bifurcates to a saddle lying on the axis of the jet, plus two stable nodes lying symmetrically to either side of the axis. At a Reynolds number of 10.09089 the pattern bifurcates a second time to form a saddle and two stable foci. Two points should be made here. The first is that the diagrams in Figure 19 depict the behavior of (40) at Reynolds numbers that lie outside of its region of validity, although one may expect the nonlinear solution to behave in a similar fashion. The second point is that the rollup of particle trajectories depicted in Figure 19*c* occurs *entirely without any local concentration of vorticity*.

It is of interest to speculate on the high-Reynolds-number (non-axisymmetric) flow from a point momentum source. In Section II we saw a model of the plane mixing layer by Corcos (1979) in which the flow was treated as deterministic at all scales. For the mixing layer, dimensional analysis leads to $\delta \sim t$, $\lambda \sim t^{1/2}$, $\eta \sim t^{1/4}$. The disparity between large and small scales increases with time. It is not obvious that in the face of such a dynamic the small scales can retain their identity for any significant length of time. However, in the case of the three-dimensional jet all three scales vary like $t^{1/2}$. The flow is self-similar at all scales. This suggests that there ought to exist a high-Reynolds-number solution which is enormously complex (with critical points in a three-dimensional phase space) but wholly deterministic and which would mimic all of the important features (spreading rate, entrainment rate, dissipation at small scales, etc) of a fully turbulent jet.

Entrainment diagrams can be worked out for a wide variety of flows including those listed in Table 2. Figure 20 illustrates three examples. Figure 20*c* shows the entrainment diagram for the Oseen vortex, an explicitly unsteady flow in the variable $r/\sqrt{\nu t}$. Figures 20*a* and *b* show entrainment diagrams derived from the stationary mean-velocity profiles of the plane turbulent mixing layer and plane turbulent jet (Cantwell 1979). Both of these flows can be formulated as self-similar in time. Normally they are measured by a laboratory observer who takes a long time average at a fixed position in physical coordinates (x, y) with the mean profiles illustrated in Figure 20, the empirically measured result. However, it is clear that another kind of average is possible. Operationally this would be a long time average referred to a receding observer who looks at the flow quite literally through the zoom lens of a camera. The rate of zoom is adjusted to match the global parameter that governs the motion and the averaging time of the experiment is limited by the physical size of the apparatus that contains the flow. Fluctuations in the evolving flow are assumed to follow the same time scale as the coherent motion and are averaged out by the receding observer. Given the complexity of the entrainment diagram for the round jet, one may conjecture that, in general, entrainment diagrams based on through-the-zoom-lens averaging will exhibit a rich structure not found in the average referred to a fixed laboratory observer.

The entrainment diagram has several useful features. It gives a compact, invariant, visual impression of the flow pattern with easily accessible information about the motion of fluid particles. The dominant physical picture of eddies as spirals comes through in the well-defined form of stable foci. The entrainment diagram can be used to analyze the dynamics of fluid motion, revealing, in some cases, a

dependence on Reynolds number that may remain hidden in a pattern of streamlines. The correspondence between the near-wall structure of the entrainment diagram for the spot (Figure 11*c*), and the space-time correlation results of Wygnanski et al (Figure 11*b*) suggests that both methods somehow focus on the same energetic motions in the flow. The prospect that space-time correlation measurements could be connected to flow variables through critical points in the entrainment diagram is an intriguing possibility that needs further study. Perhaps some hint for approaching this issue can be found in the vector field of correlations introduced by Willmarth & Wooldridge (1963).

VI CONCLUDING REMARKS

Our understanding of the physics of turbulent motion has increased tremendously in recent years. The major new fact is that turbulence is characterized by a remarkable degree of order. But along with order has come new complication for it appears that many turbulent flows retain a permanent imprint of their infinitely variable initial state. Approximately twenty years have passed since the earliest observations of organized structure. Yet progress in incorporating this structure into practical engineering methods has been slow and the connection to a truly predictive theory has not yet been made. Turbulence remains a major unsolved problem of classical physics.

ACKNOWLEDGMENT

I would like to express thanks to Garry Brown, Luis Bernal, and John Konrad who were involved in various aspects of making the film used for the animation of vortex pairing. I would also like to acknowledge the support of NASA Ames Research Center under NASA Grant NSG2392.

Literature Cited

Abernathy, F. H., Kronauer, R. E. 1962. The formation of vortex streets. *J. Fluid Mech.* 13:1–20

Ashurst, W. T. 1977. Numerical simulation of turbulent mixing layers via vortex dynamics. *Sandia Lab. Rep. SAND 77-8612*

Bakewell, H. P., Lumley, J. L. 1967. Viscous sublayer and adjacent region in turbulent pipe flow. *Phys. Fluids* 10:1880–89

Batt, R. G. 1975. Some measurements on the effect of tripping the two-dimensional shear layer. *AIAA J.* 13:245–47

Bevilaqua, P. M., Lykoudis, P. S. 1971. Mechanism of entrainment in turbulent waves. *AIAA J.* 9:1657–59

Birch, S. 1980. *Evaluation of Shear-Layer Data—Rep. to the Organizing Committee, 1980–81 Conf. on Computation of Complex Turbulent Flows*. Stanford Univ.

Blackwelder, R. F. 1978. The bursting process in turbulent boundary layers. *Lehigh Workshop on Coherent Structure in Turbulent Boundary Layers*. ed. C. R. Smith, D. E. Abbott, pp. 211–27

Blackwelder, R. F., Eckelmann, H. 1979. Streamwise vortices associated with the bursting phenomenon. *J. Fluid Mech.* 94:577–94

Blackwelder, R. F., Kaplan, R. E. 1971. Intermittent structures in turbulent boundary layers. *AGARD Conf. Proc. No. 43*, London, 5-1/5-7

Blackwelder, R. F., Kovasznay, L. S. G. 1972. Time scales and correlations in a turbulent boundary layer. *Phys. Fluids* 15:1545–54

Bouchard, G. E., Reynolds, W. C. 1978. Control of vortex pairing in a round jet. *Bull. Am. Phys. Soc.* 23(8):1013

Boussinesq, J. 1877. Théorie de l'écoulement tourbillant. *Mém. Prés. Acad. Sci.* 23:46

Briedenthal, R. E. 1978. *A chemically reacting turbulent shear layer*. PhD thesis. Calif. Inst. Tech., Pasadena, Calif.

Brown, G. L., Roshko, A. 1974. On density effects and large structure in turbulent mixing layers. *J. Fluid Mech.* 64:775–816

Brown, G. L., Thomas, A. S. W. 1977. Large structure in a turbulent boundary layer. *Phys. Fluids* 20(10):S243–52

Cantwell, B. J. 1978. Similarity transformations for the two-dimensional unsteady stream function equation. *J. Fluid Mech.* 85:257–71

Cantwell, B. J. 1979. Coherent turbulent structures as critical points in unsteady flow. *Arch. Mech. Stosow.* 31:707–21

Cantwell, B. J. 1980. Transition in the axisymmetric jet. (*SUDAAR*) *Rep. No. 521*, Stanford Univ., Dept. Aeronaut. and Astronaut. *J. Fluid Mech.* In press

Cantwell, B. J., Coles, D. E., Dimotakis, P. E. 1978. Structure and entrainment in the plane of symmetry of a turbulent spot. *J. Fluid. Mech.* 87:641–72

Chandrasekhar, S. 1949. On Heisenberg's elementary theory of turbulence. *Proc. R. Soc. London Ser. A.* 200:20–33

Chandrasuda, C., Mehta, R. D., Weir, A. D., Bradshaw, P. 1978. Effect of free shear stream turbulence on large structure in turbulent mixing layers. *J. Fluid Mech.* 85:693–704

Chapman, D. R. 1979. Computational aerodynamics development and outlook. *AIAA Dryden Lect. 79-0129*

Chorin, A. J., Bernard, P. S. 1973. Discretization of a vortex sheet with an example of roll-up. *J. Comput. Phys.* 13:423–29

Clark, R., Ferziger, J. H., Reynolds, W. C. 1979. Evaluation of subgrid-scale models using an accurately simulated turbulent flow. *J. Fluid Mech.* 91:1–16

Clements, R. R. 1973. An inviscid model of two-dimensional vortex shedding. *J. Fluid Mech.* 57:321–36

Coles, D. E. 1956. The law of the wake in the turbulent boundary layer. *J. Fluid Mech.* 1:191–226

Coles, D. E. 1978. A model for the flow in the viscous sublayer. *Lehigh Workshop on Coherent Structure in Turbulent Boundary Layers*, ed. C. R. Smith, D. E. Abbott, pp. 462–75

Coles, D. E., Barker, S. J. 1975. Some remarks on a synthetic turbulent boundary layer. In *Turbulent Mixing in Nonreactive and Reactive Flows*, ed. S. N. B. Murthy, pp. 285–92

Coles, D. E., Van Atta, C. W. 1967. Digital experiment in spiral turbulence. *Phys. Fluids Suppl. Part II* 10:S120–21

Corcos, G. 1979. The mixing layer: deterministic models of a turbulent flow. *Dept. Mech. Engrg. Rep. No. FM-79-2*. Univ. California, Berkeley

Corino, E. R., Brodkey, R. S. 1969. A visual investigation of the wall region in turbulent flow. *J. Fluid Mech.* 37:1–30

Corrsin, S. 1943. Investigations of flow in an axially symmetric heated jet of air. *NACA Adv. Conf. Rep. 3123*

Corrsin, S., Kistler, A. 1954. The free stream boundaries of turbulent flows. *NACA Tech. Note No. 3133* (also *NACA Tech. Rep. No. 1244*, 1955)

Crow, S. C., Champagne, F. H. 1971. Orderly structure in jet turbulence. *J. Fluid Mech.* 48:547–91.

Davies, M. E. 1976. A comparison of the wake structure of a stationary and oscillating bluff body, using a conditional averaging technique. *J. Fluid Mech.* 75:209–23

Dimotakis, P. E., Brown, G. L. 1976. The mixing layer at high Reynolds number: large structure dynamics and entrainment. *J. Fluid Mech.* 78:535–60

Dinkelacker, A., Hessel, M., Meier, G., Schewe, G. 1977. Investigation of pressure fluctuations beneath a turbulent boundary layer by means of an optical method. *Phys. Fluids* 20(10):S216–24

Elder, J. W. 1960. An experimental investigation of turbulent spots and breakdown to turbulence. *J. Fluid Mech.* 9:235–46

Emmons, H. W. 1951. The laminar-turbulent transition in a boundary layer. Part I. *J. Aeronaut. Sci.* 18:490–98

Falco, R. E. 1977. Coherent motions in the outer region of turbulent boundary layers. *Phys. Fluids* 20(10):5124–32

Favre, A. J., Gaviglio, J. J., Dumas, R. 1957. Space-time double correlation and spectra in a turbulent boundary layer. *J.*

Fluid Mech. 2:313–41
Freymuth, P. 1966. On transition in a separated boundary layer. *J. Fluid Mech.* 25:683–704
Furuya, Y., Osaka, H. 1976. *Three-dimensional structure of nominally two-dimensional turbulent boundary layer*. Presented at the 14th IUTAM Congress, Delft. *Abstr. No. 160*
Gad-el-Hak, M., Blackwelder, R. F. 1979. A visual study of the growth and entrainment of turbulent spots. *Proc. IUTAM Symp. on Transition*, Stuttgart, Germany
Grant, H. L. 1958. The large eddies of turbulent motion. *J. Fluid Mech.* 4:149–90
Grass, A. J. 1971. Structural features of turbulent flow over smooth and rough boundaries. *J. Fluid Mech.* 50:223–56
Griffin, O. M., Ramberg, S. E. 1974. The vortex street wakes of vibrating cylinders. *J. Fluid Mech.* 66:553–78
Gupta, A. K., Laufer, J., Kaplan, R. E. 1971. Spatial structure in the viscous sublayer. *J. Fluid Mech.* 50:493–512
Hama, F. R., Nutant, J. 1963. Detailed flow field observations in the transition process in a thick boundary layer. *Proc. 1963 Heat Transfer and Fluid Mech. Inst.*, pp. 77–94
Hanratty, T. J., Chorn, L. G., Hatziavramidis, D. T. 1977. Turbulent fluctuations in the viscous wall region for Newtonian and drag reducing fluids. *Phys. Fluids* 20(10):S112–19
Head, M. R., Bandyopadhyay, P. 1978. Combined flow visualization and hot wire measurements in turbulent boundary layers. *Lehigh Workshop on Coherent Structure in Turbulent Boundary Layers*, ed. C. R. Smith, D. E. Abbott, pp. 98–129
Heisenberg, W. 1948a. Zur statistischen theorie der turbulenz. *Z. Phys.* 124:628–57
Heisenberg, W. 1948b. On the theory of statistical and isotropic turbulence, *Proc. R. Soc. London Ser. A* 195:402–6
Hinze, J. O. 1959. *Turbulence*. New York: McGraw-Hill. 1st ed.
Hunt, J. C. R., Abell, C. J., Peterka, J. A., Woo, H. 1978. Kinematic studies of the flows around free or surface mounted obstacles; applying topology to flow visualization. *J. Fluid Mech.* 86:179–200
Hussain, A. K. M. F., Reynolds, W. C. 1975. Measurements in fully developed turbulent channel flow. *J. Fluid Engrg.* 97:568–80
Hussain, A. K. M. F., Zaman, K. B. M. Q. 1978. The free shear layer tone phenomenon and probe interference. *J. Fluid Mech.* 87:349–84
Kim, H. T., Kline S. J., Reynolds, W. 1971. The production of the wall region in turbulent flow. *J. Fluid Mech.* 50:133–60
Klebanoff, P. S. 1954. Characteristics of turbulence in a boundary layer with zero pressure gradient. *NACA Tech. Note No. 3178*
Kline, S. J. 1978. The role of visualization in the study of the structure of the turbulent boundary layer. *Lehigh Workshop on Coherent Structure of Turbulent Boundary Layers*, ed. C. R. Smith, D. E. Abbott, pp. 1–26
Kline, S. J., Falco, R. E. 1980. Summary of the AFOSR/MSU research specialists workshop on coherent structure in turbulent boundary layers. *AFOSF-TR-80-0290 ADA 083717*
Kline, S. J., Runstadler, P. W. 1959. Some preliminary results of visual studies of the flow model of the wall layers of the turbulent boundary layer. *Trans. ASME (Ser. E)* 2:166–70
Kline, S. J., Reynolds, W. C., Schraub, F. A., Runstadler, P. W. 1967. The structure of turbulent boundary layers. *J. Fluid Mech.* 30:741–73
Kolmogorov, A. N. 1941. The local structure of turbulence in incompressible flow for very large Reynolds number. *C. R. Acad. Sci. U.R.S.S.* 30:301
Kovasznay, L. S. G. 1948. Spectrum of locally isopropic turbulence. *J. Aeronaut. Sci.* 15:745–53
Kovasznay, L. S. G., Kibens, V., Blackwelder, R. 1970. Large scale motion in the intermittent region of a turbulent boundary layer. *J. Fluid Mech.* 41:283–325
Laufer, J. 1954. The structure of turbulence in fully developed pipe flow. *NACA Tech. Note No. 2954*
Laufer, J., Narayanan, M. A. B. 1971. Mean period of the turbulent production mechanism in a boundary layer. *Phys. Fluids* 14:182–83
Lee, M. K., Eckelmann, L. D., Hanratty, T. J. 1974. Identification of turbulent wall eddies through the phase relation of the components of the fluctuating velocity gradient. *J. Fluid Mech.* 66:17–34
Leonard, A. 1979. Vortex simulation of three-dimensional, spotlike disturbances in a laminar boundary layer. *NASA Tech. Memo. 78579* (also in *Turbulent shear flows II*, ed. L. J. S. Bradbury, pp. Berlin:

Springer 67:77
Liepmann, H. W. 1952. Aspects of the turbulence problem. *J. Appl. Math. and Phys.* (*ZAMP*) 3:321–426
Liepmann, H. W. 1962. Free turbulent flows. In *Colloques Internationaux du Centre National de la Recherche Scientifique* (*C.N.R.S.*), *Mechnique de la Turbulence, Marseilles*, 108:211–27
Liepmann, H. W. Laufer, J. 1947. Investigation of free turbulent mixing. *NACA Tech. Note No. 1257*
Lighthill, M. J. 1963. In *Laminar Boundary Layers*, ed. L. Rosenhead, pp. 48–88. Oxford Univ. Press
Lindgren, E. R. 1969. Propagation velocity of turbulent slugs and streaks in transition pipe flow. *Phys. Fluids* 12:418–25
Lu, S. S., Willmarth, W. W. 1973. Measurements of the Reynolds stress in a turbulent boundary layer. *J. Fluid Mech.* 60:481–511
Lugt, H. J. 1979. The dilemma of defining a vortex. In *Recent Developments in Theoretical and Experimental Fluid Mechanics*, ed. U. Muller, K. G. Roesner, B. Schmidt, pp. 309–21. Berlin/Heidelberg/New York: Springer
Meijer, M. C. 1965. Pressure measurements on flapped hydrofoils in cavity flows and wake flows. *Hydrodyn. Lab. Rep. No. E-133.2*. Calif. Inst. Tech.
Mitchner, M. 1954. Propagation of turbulence from an instantaneous point disturbance. *J. Aeronaut. Sci.* 2(5):350–51
Moin, P., Reynolds, W. C., Ferziger, J. H. 1978. Large eddy simulation of incompressible turbulent channel flow. *Dept. Mech. Engrg. Rep.* 91:1–16. Stanford Univ.
Narayanan, B., Marvin, J. 1978. On the period of the coherent structure in boundary layers at large Reynolds numbers. *Lehigh Workshop on Coherent Structure in Turbulent Boundary Layers*, ed. C. R. Smith, D. E. Abbot, pp. 380–86
Nychas, S. G., Hershey, H. C., Brodkey, R. S. 1973. A visual study of turbulent shear flow. *J. Fluid Mech.* 61:513–40
Offen, G. R., Kline, S. J. 1974. Combined dye-streak and hydrogen-bubble visual observations of a turbulent boundary layer. *J. Fluid Mech.* 62:223–39
Offen, G. R., Kline, S. J. 1975. A proposed model of the bursting process in turbulent boundary layers. *J. Fluid Mech.* 70:209–28
Oldaker, D. K., Tiederman, W. G. 1977. Spatial structure of the viscous sublayer in drag reducing channel flows. *Phys. Fluids* 20(10): *S*133–44
Onsager, L. 1945. The distribution of energy in turbulence. *Phys. Rev. Abstr.* 68:286
Onsager, L. 1949. Statistical hydrodynamics. *Nuovo Cimento Suppl.* 6:279–87
Oster, D., Wygnanski, I., Dziomba, B., Fiedler, H. 1977. On the effect of initial conditions on the two dimensional turbulent mixing layer. In *Lecture Notes in Physics, Vol. 75*, p. 48. Berlin: Springer (*Structure and Mechanisms of Turbulence I*, ed. H. Fiedler)
Oswatitsch, K. 1958. *Die Ablösungsbedingung von Grenzschichten*, Grenzschicht Forschung, ed. H. Goertler, pp. 357–67. Berlin/New York: Springer
Owen, F. K., Johnson, D. A. 1978. Measurements of unsteady vortex flow fields. *AIAA Paper 78–18*
Payne, F. R., Lumley, J. L. 1967. Large eddy structure of the turbulent wake behind a circular cylinder. *Phys. Fluids Suppl.* 10:S194–96
Peake, D., Tobak, M. 1980. Three-dimensional interactions and vortical flows with emphasis on high speeds. *NASA Tech. Memo. 81169*
Perry, A. E., Lim, T. T. 1978. Coherent structures in coflowing jets and wakes. *J. Fluid Mech.* 88:451–64
Perry, A. E., Lim T. T. 1978. Coherent structures in coflowing jets and wakes. *J. Fluid Mech.* 88:451–64
Perry, A. E., Watmuff, J. H. 1979. The phase-averaged large-scale structures in three-dimensional turbulent wakes. *Dept. Mech. Rep. FM-12*. Univ. Melbourne
Perry, A. E., Lim, T. T., Chong, M. S., Teh, E. W. 1980. The fabric of turbulence. *AIAA Pap. 80-1358*
Perry, A. E., Lim, T. T., Chong, M. S. 1980. Instantaneous vector fields in coflowing jets and wakes. *J. Fluid Mech.* In press
Prandtl, L. 1925. Bericht uber untersuchungen zur ausgebildeten turbulenz. *Z. Angew. Math. Mech.* 5:136–39
Praturi, A. K., Brodkey, R. S. 1978. A stereoscopic visual study of coherent structures in turbulent shear flow. *J. Fluid Mech.* 89:251–72
Pullin, D. I. 1978. The large-scale structure of unsteady self-similar rolled-up vortex sheets. *J. Fluid Mech.* 80:401–30
Rao, K. N., Narasimha, R., Narayanan, M. A. B. 1971. Bursting in a turbulent boundary layer. *J. Fluid Mech.* 48:339–52
Reynolds, O. 1895. On the dynamical the-

ory of incompressible viscous fluids and the determination of the criterion. *Philos. Trans. R. Soc. London Ser. A* 186:123

Reynolds, W. C. 1976. Computation of turbulent flows. *Ann. Rev. Fluid Mech.* 8:183–208

Roshko, A. 1976. Structure of turbulent shear flows: a new look. Dryden Research Lecture. *AIAA J.* 14:1349–57

Sabot, J., Saleh, I., Comte-Bellot, G. 1977. Effects of roughness on the intermittent maintenance of Reynolds shear stress in pipe flow. *Phys. Fluids* 20(10):S150–55

Saffman, P. G., Baker, G. R. 1979. Vortex interactions. *Ann. Rev. Fluid Mech.* 11:95–122

Sarpkaya, T. 1975. An inviscid model of two-dimensional vortex shedding for transient and asymptotically steady separated flow over an inclined flat plate. *J. Fluid Mech.* 68:109–28

Savas, O. 1979. *Some measurements in synthetic turbulent boundary layers*. PhD thesis. Calif. Inst. Tech., Pasadena, Calif.

Schubauer, G. B., Klebanoff, P. S. 1955. Contributions on the mechanics of boundary layer transition. *NACA Tech. Note No. 3489* (See also *NACA Tech. Rep. No. 1289*, 1956)

Smith, C. R. 1978. Visualization of turbulent boundary layer structure using a moving hydrogen bubble wire probe. *Lehigh Workshop on Coherent Structure in Turbulent Boundary Layers*, ed. C. R. Smith, D. E. Abbott, pp. 48–97

Sozou, C. 1979. Development of the flow field of a point force in an infinite fluid. *J. Fluid Mech.* 91:544–54

Spalding, D. B. 1961. A single formula for the law of the wall. *J. Appl. Mech.* 28:455–57

Spencer, B. W., Jones, B. G. 1971. Statistical investigation of pressure and velocity fields in the turbulent two-stream mixing layer. *AIAA Pap. No. 71-613*

Taylor, G. I. 1915. Eddy motions in the atmosphere. *Philos. Trans. R. Soc. London Ser. A* 215:1–26

Taylor, G. I. 1932. Note on the distribution of turbulent velocities in a fluid near a solid wall. *Proc. R. Soc. London Ser. A* 135:678–84

Taylor, G. I. 1935. The statistical theory of turbulence, Parts I–IV, *Proc. R. Soc. London Ser. A* 151:421–511

Theodorsen, T. 1955. The structure of turbulence. In *50 Jahre Grenzschichtforsung*, ed. H. Görtier, W. Tollmein, p. 55. Braunschweig, Veiweg & Sohn

Townsend, A. A. 1947. Measurements in the turbulent wake of a cylinder. *Proc. R. Soc. London Ser. A* 190:551–61

Townsend, A. A. 1956. *The Structure of Turbulent Shear Flow*. Cambridge Univ. Press. 1st ed.

Townsend, A. A. 1970. Entrainment and the structure of turbulent flow. *J. Fluid Mech.* 41:13–46

Townsend, A. A. 1976. *The Structure of Turbulent Shear Flow*. Cambridge Univ. Press. 2nd ed.

Tu, B. J., Willmarth, W. W. 1966. An experimental study of turbulence near the wall through correlation measurements in a thick turbulent boundary layer. *Tech. Rep. No. 02920-3-T*. Dept. Aerosp. Engrg., Univ. Michigan, Ann Arbor

Turner, J. S. 1964. The flow into an expanding spherical vortex. *J. Fluid Mech.* 18:195–208

Von Weizsäcker, C. F. 1948. Das spectrum der turbulenz bei grossen Reynolds-Schen zahlen. *Z. Phys.* 124:614–27

Willmarth, W. W. 1975. Pressure fluctuations beneath turbulent boundary layers. *Ann. Rev. Fluid Mech.* 7:13–37

Willmarth, W. W., Bogar, T. J. 1977. Survey and new measurements of turbulent structure near the wall. *Phys. Fluids* 20(10):S9–21

Willmarth, W. W., Lu, S. S. 1972. Structure of the Reynolds stress near the wall. *J. Fluid Mech.* 55:65–69

Willmarth, W. W., Wooldridge, C. E. 1962. Measurements of the fluctuating pressure at the wall beneath a thick turbulent boundary layer, *J. Fluid Mech.* 14:187–210

Willmarth, W. W., Wooldridge, C. E. 1963. Measurements of the correlation between the fluctuating velocities and the fluctuating wall pressure in a thick turbulent boundary layer. *AGARD Rep. 456*

Willmarth, W. W., Yang, C. S. 1970. Wall pressure fluctuations beneath turbulent boundary layers on a flat plate and a cylinder. *J. Fluid Mech.* 41:47–80

Winant, C. D., Browand, F. K. 1974. Vortex pairing, the mechanism of turbulent mixing layer growth at moderate Reynolds number. *J. Fluid Mech.* 63:237–55

Wygnanski, I., Fiedler, H. E. 1970. The two dimensional mixing region, *J. Fluid Mech.* 41:327–61

Wygnanski, I. J., Champagne, F. H. 1973.

On transition in a pipe. Part I. The origin of puffs and slugs and the flow in a turbulent slug. *J. Fluid Mech.* 59:281–335

Wygnanski, I. J., Sokolov, N., Friedman, D. 1976. On the turbulent "spot" in a boundary layer undergoing transition. *J. Fluid Mech.* 78:785–819

Wygnanski, I., Haritonidis, J. H., Kaplan, R. E. 1979. On a Tollmien-Schlichting wave packet produced by a turbulent spot. *J. Fluid Mech.* 92:505–28

Zakkay, V., Barra, V., Wang, C. R. 1978. Coherent structure of turbulence at high subsonic speeds. *Lehigh Workshop on Coherent Structure in Turbulent Boundary Layers*, ed. C. R. Smith, P. E. Abbott, pp. 387–95

Zilberman, M., Wygnanski, I., Kaplan, R. E. 1977. Transitional boundary layer spot in a fully turbulent environment. *Phys. Fluids* 20(10):S258–71